Robust Controller for the Bosch SCARA Robot

May 1995
G.E.Smid
A.95.017(682)

SCARA

ROBUST CONTROL

Designing and Analysing a Robust Controller for the Bosch SCARA

An Application of Robust Control on a Robot

G.E.Smid

April 1994

Supervisor Prof. ir. G. Honderd
Mentors dr.ir. T.J.J. van den Boom
dr.ir. W. Jongkind
ir. S. Stramigioli

Delft University of Technology
Department of Electrical Engineering
Control Laboratory

List of Symbols

L_{mi}	Inductance of motor coil of joint i	$[H]$
L_i	Size of the Link i	$[H]$
R_{mi}	Impendance of motor armature, included wires of joint i	$[\Omega]$
K_{mi}	Servo motor constant of joint i	$[Nm/A]$
J_{mi}	Inertia of servo motor of joint i	$[kgm^2]$
J_{Li}	Inertia of the Link i	$[kgm^2]$
J_i	Total inertia of Link i	$[kgm^2]$
J_c	Cross-coupling inertia between joints	$[kgm^2]$
F_{vi}	Viscous friction of joint i	$[Nms/rad]$
F_{vL}	Viscous friction in mechanical link 1	$[Nms/rad]$
F_{vm}	Viscous friction in Servo motor of joint 1	$[Nms/rad]$
F_{ci}	Coulomb friction of joint i	$[Nm]$
F_{si}	Static friction (Stiction) of joint i	$[Nm]$
K_{Pi1}	Proportional constant of tacho controller in Servo Amplifier i	$[1]$
K_{Ii1}	Integration constant of tacho controller in Servo Amplifier i	$[s^{-1}]$
K_{Pi2}	Proportional constant of current controller in Servo Amplifier i	$[V/A]$
K_{Ii2}	Integration constant of current controller in Servo Amplifier i	$[V/As]$
τ_i	Time constant of Tacho controller in Servo Amplifier i	$[s^{-1}]$
m_l	Load mass	$[kg]$
K_S	Spring constant	$[Nm/rad]$
D_S	Damper constant	$[Nms/rad]$
θ_{mi}	Position of motor axis of joint i	$[rad]$
θ_i	Position of joint axis i	$[rad]$
$\dot{\theta}_{mi}$	Velocity of motor axis of joint i	$[rad/s]$
$\dot{\theta}_i$	Velocity of joint axis i	$[rad/s]$
$\ddot{\theta}_i$	Acceleration of joint axis i	$[rad/s^2]$
N_1	Gear ratio	$[1]$
$\tau_{LD,i}$	Disturbance torques on joint i	$[Nm]$
δ_{ADi}	Quantization error of sensor joint i	$[rad]$
δ_{DA}	Resolution of DA-converter	$[V]$
δ_F	Perturbation in friction	$[Nms/rad]$
$\delta_{1/J}$	Perturbation in inertia	$[1/kgm^2]$
δ_θ	Tracking error	$[rad/s]$

p_1	Interconnection output to inertia error	$[Nm]$
p_2	Interconnection output to friction error	$[rad/s]$
q_1	Interconnection intput to inertia error	$[N/kgm]$
q_2	Interconnection intput to friction error	$[Nm]$
U_S	Input voltage to Servo motor	$[V]$
U_{SA}	Input voltage to Tacho controller of Amplifier System	$[V]$
I_{SA}	Input current to Current controller of Amplifier System	$[A]$
h	Sample time	$[s]$
W_Δ	Scaling function for perturbation matrix	
W_P	Weighing function of tracking error (Performance Spec)	
W_θ	Scaling function for velocity setpoint	
W_τ	Scaling function for disturbance torque	
W_{DA}	Scaling function for Amplifier setpoint	
W_F	Scaling of Friction perturbation	
W_J	Scaling of inertia perturbation	
K	Controller	
$\boldsymbol{B}$	Set of all normed perturbation matrices Δ with $\sigma_{\max}(\Delta) \leq 1$	
M	Closed-loop interconnection matrix	
M'	Open-loop interconnection matrix	
Δ	Noise-block, built of Δ_1 and Δ_P	
Δ_1	Perturbation transfer matrix (structured)	
Δ_P	Blockstructure appended to Δ for robust performance calculations	
d	Input signals	
e	Tracking error	
c	Controller signal	
w	Input of perturbation matrix Δ_1 into the interconnection matix	
z	Output of the interconnection matix to the perturbation matrix Δ_1	

Preface

This thesis describes the application of Robust Control on a robot arm. The Robot group of the Control Laboratory takes part in the DIAC[1] project in which members of four departments cooperate with the aim of creating a flexible assembly cell.

This research project concerned with this thesis, is an investigation to the analysis of the robustness in performance of the Bosch SCARA[2], one of the two robots in the DIAC. It involves the uncertainty modelling of the control system and the composition of the so called Linear Fractional Transformation. A performance specification should be posed and mathematical analysis can give insight of the ability of the perturbed system to perform accordingly.

The reader should be aquainted with mechanical and mechatronical systems and their physical behaviour, as well as a basic knowledge of control theory. Modelling and Identification involve an important part of the report. The introduction on Robust Control theory, together with the chapter explaining the analysis of the system in the focus of Robust Control, could be read by those who are unfamiliar with the area but who like to learn about it. It also could be an introduction to students of the Control Laboratory who want to do a similar research or who want to extend it.

With this thesis work, I will finish my study on Electrical Engineering at the Delft University of Technology. I would like to thank my mentors T.T.J. van den Boom, who allways had the time for my questions, even when he was very busy, and W. Jongkind, with whom I might have spend more time, discussing society than control theory, and S. Stramigioli, who helped me a lot on the physical understanding of the mechanical system. Above all, I would like to thank professor G. Honderd for his enthausiasm and engagement in my occupation, as he is with all of his students.

Delft, May 10th 1995

G.E. Smid

[1] DIAC stands for Delft Intelligent Assembly Cell

[2] SCARA means Selective Complience Assembly Robot Arm

Contents

Chapter 1

Introduction

Control system design can be devided into two areas of interest. Thefirst one focuses on gaining maximum performance. The other area iswhere it comes to safety and minimum error boundaries.No design method can tackle all the issues that have to be studiedwhen making a real world design. Typically a synthesis method willfocus on one or two issues and leave others to the designer's commonsense as often hidden conditions. Robustness, i.e. maintainingsystem performance in the presence of variations of the systemdynamics, is an important property of a good controller, sincecontrollers often are designed using approximated or estimated models . The H_∞-control theory focusses on the uncertaintyaspect and finds a controller with "optimal" robustness.In the case of this thesis project, the design problem focusses onthe first two joints of the Bosch SCARA. The control problem for thereport is

Analysing the Bosch SCARA control system with severalcontrollers by applying μ-analysis on the Linear FractionalTransformation of it's model.

This problem incorporates the two areas of controlengineering together. Robust control aims primarely on the safetyof the control system. In all situations in which small errors cancause great impact or damage, it is most important to control safelyand accurately, more than it is to control fast.In the DIAC project, the cooperation of two robots demand from acontroller a guarantee, concerning limits on the error. For thisresearch, the first two joints that move the robot in thehorizontal plane are treated. Therefore the coupling will beconsidered as a disturbing interaction bet ween the two joints. Also perturbations of the torques are taken into account. There aremany more small errors in the model, but in this report they are notconsidered. Figure 1.1 shows the control environment ofthe first two joints, with most of the disturbing and perturbinginfluences.In the process of identification for the disturbing signals, a globalupperbound in size will be estimated. For the perturbed parameterswe will identify a nominal value, and a value for the maximum sizeof the deviation from that nominal value. A nominal model withoutdisturbance is created, with a separate multivariable feedback loopcontaining all the perturbations and parameter uncertainties. Thephylosophy is that the loopgain of this loop should be less than 1.This criterion characterizes the system's robust stability. In thepresence of robust stability, we are able to define a maximum sizeof

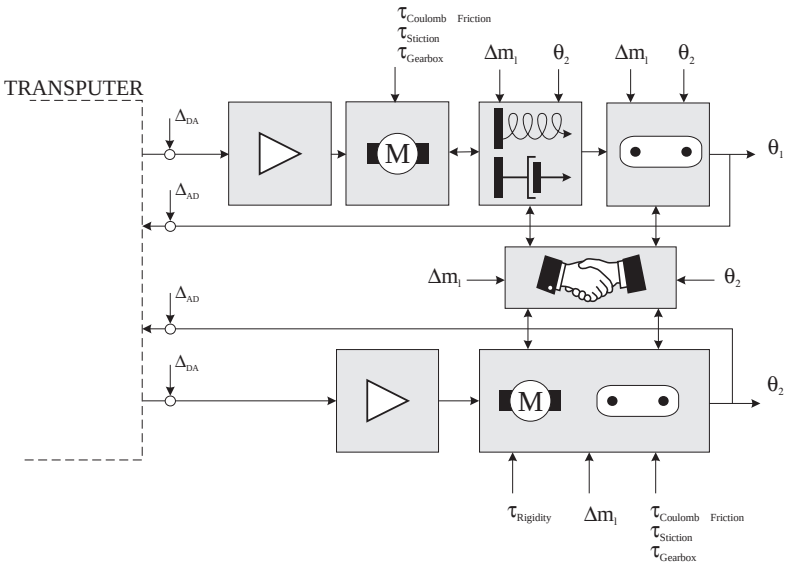

Figure 1.1: *Modular presentation of the control system of the first two joints of the Bosch SCARA, with the emphasis on the disturbing influences.*

the tracking error. A system satisfies robust performance, if themaximum occuring tracking error stays below our performancecriterion, often referred to as the performance specification, forall the possible disturbances.The maximum boundaries of the model perturbations imply that thecomplete set of possible models within the posed interval isallowed. Seldom however, the model will deviate so far from it'snominal state as the maximum boundaries allow it to do, and inmost cases the system could gain better performance if a controllerwould be implemented, based on the nominal model withoutperturbation. However such a controller will not enable the systemto perform well in all circumstances and therefore lose robustperformance. The result is that often a conservative control law iscalculated for a system to let it have robust performance. As muchinformation as possible will be needed from the system to let this benot a too big problem. This report will start with the identification of the real system.From the beginning it is important to realize that accurateinformation is need ed from the deviations from the nominal model.Therefore in the first chapter on the identification and modelling,a section is devoted to the model perturbations.

To be able tocontinue the modelling in the focus of Robust Control, moreinformation is needed about the designing strategy and themathematical background, the theory is concerned with. Therefore acomplete chapter is devoted to the explanation of Robust Controltheory. This will conclude with a mathematical tool calledμ-analysis with which the Robust Performance of a perturbedsystem can be analysed.

With this knowledge we can continue ourquest for the Holy Grail. The identified model will be remodelledtowards a Linear Fractional Transformation. This means that we dealwith a well-known linear nominal model with a multivariableperturbation feedback loop. The nominal system is then des cribedin state space matrices and for all input and output signals,weighting functions will be defined, using the

knowledge of theidentification in the beginning. This part will conclude with thedefinition of an interconnection matrix of each joint, ready forusing in the Robust Control μ-toolbox of MATLAB.
The following chapter is devoted to the robustness analysis of thesystem and to the development of a robust controller. First, somecontrol design strategies are discussed and then the original modelsof the SCARA will be exposed to the μ-analysis. Finally acontroller will be generated with the μ software and theclosed-loop system will be analysed, too . Allways the performancewill be subjected to the stability criterion. So if robust stabilityis not established, we have to decrease our performancespecification or redesign the controller or tighten constraintson perturbations and analyse again.
This last chapter will be followed by theconclusions and recommandations. An important notion can be drawn from this thesis work in thereal-life engineering. This is that a lot of research has to be doneon modelling and identification of nominal and perturbational valuesof every facet of the system. This research is then only thepreparation for the μ-analysis, so after that time the engineeris merely able to analyse the existing system from the robustcontrol point of view. Try to imagine the costs of the time consuming a research performed in a company.

Chapter 2

Identification

System identification deals with the problem of estimating parameters of dynamical systems, based on observed data from the system. It is necessary to use a model that describes the relationship among the system variables in terms of a mathematical expression like a difference or differential equation. Often this kind of model is characterized by a number of adjectives (time continuous, disturbed, deterministic or stochastic, linear or non-linear).

In this chapter a model of the first two axes will be derived in the form of a block diagram. The parameters of the model will be identified and, in the aim of a robust control model, an extensive investigation of uncertainties or perturbations of signals and nominal values of the identified parameters is necessary. This is not a trivial task. It will be introduced at the end of this chapter and it will be the subject of chapter 3 also.

The explanation of the modelling will be preceeded by a discussion on linearity. It explaines the way to deal with a model that is not linear in the focus of Robust Control modelling. Then modelling will be started with bondgraphs of the first two servo motors, connected to the mechanical links and setpointed with currents. The current is a straightforward signal in the sence of controlling a servo motor. It is proportional to the torque on the motor armature.

Eventually, the models are implemented in SIMULINK, the simulation tool under MATLAB. Simulations with the model will be compared with measurements of the real robot-arm.

2.1 Introduction

Most of Robust Control theory makes use of design analysis ‘tools’ that are only valid for linear time invariant models. The development of a robust controller for the Bosch SCARA therefore needs an adequate linear time-invariant model of the real robot arm. The solution to this problem will not be

trivial.

For clearity the property *linear* will be explained once again. In general, a *necessary condition* for a linear system can be determined in terms of an excitation of $x(t)$ and a responce $y(t)$. When the system is at rest and it is subjected to an excitation $x_1(t)$, it provides a responce $y_1(t)$. Furthermore when the system is subjected to an excitation $x_2(t)$, it provides a corresponding responce $y_2(t)$. For a linear system it is *necessary* that the excitation $x_1(t) + x_2(t)$ results in a responce $y_1(t) + y_2(t)$. This is usually called the principle of *superposition* [Dor89].

It may be clear that most of the complex mechanical systems that include servo motors, gearboxes, dynamic coupling and a finite rigidity bare lots of non-linear effects. Figure 2.1 shows a ramp signal directly on the motor armature. It may be clear that friction effects play an important role and therefore make the system non-linear. Straightforward modelling will thus lead us to a model that is not suitable for Robust Control design. This problem can be solved by considering the non-linear effects as 'disturbances'. Together with noise signals, perturbations and parameter uncertainties they will not be a part of the white-box linear time-invariant model that is used for the design of the controller. Therefore they are wrapped together in a multivariable feedback-loop and placed outside what from now on will be called the *nominal model*. The next chapter will discuss this way of modelling again and will explain some theory on how to deal with this error-loop.

For the Bosch SCARA this consideration means that effects like static and Coulomb friction will be interpreted as errors of the nominal model. Figure 2.1 shows these effects clearly. The dashed line plots the current setpoint and the solid line plots the resulting angular velocity of the open-loop system. Clearly when the driving torque becomes small, the motor stops rotating, and starts again at a torque of certain size. A more extensive discussion on these effect follows in sections 2.3.3 and 2.4.4.

From now on, this chapter will reveal the complete model as it can be derived from the first principles of physics and from the electrical circuit diagrams of the system. Uncertain disturbances and non-linear behaviour will be extracted from the model and will be placed in seperate error-loops.

2.2 Energy distributions on the Robot Arm

In the scope of modelling a system, engineers sometimes try to derive a bond graph of a system before developing a block diagram. Bondgraphs model energy exchange between interacting elements by means of conjugate power variables of opposite direction. They represent physical relations between physical parts of the system. They need no artificial feedback loops to model interaction.

When the laws of bondgraphs are obayed, it will in almost any case result in a model that is physically a true approximation of a real system.

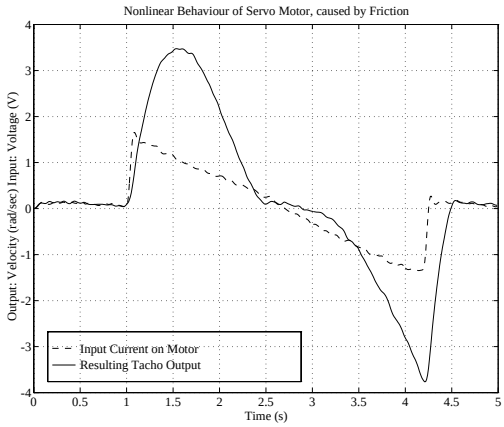

Figure 2.1: *Ramp signal straight on the motor armature. Clearly the system suffers from Non-linear friction effects near* $\omega = 0$.

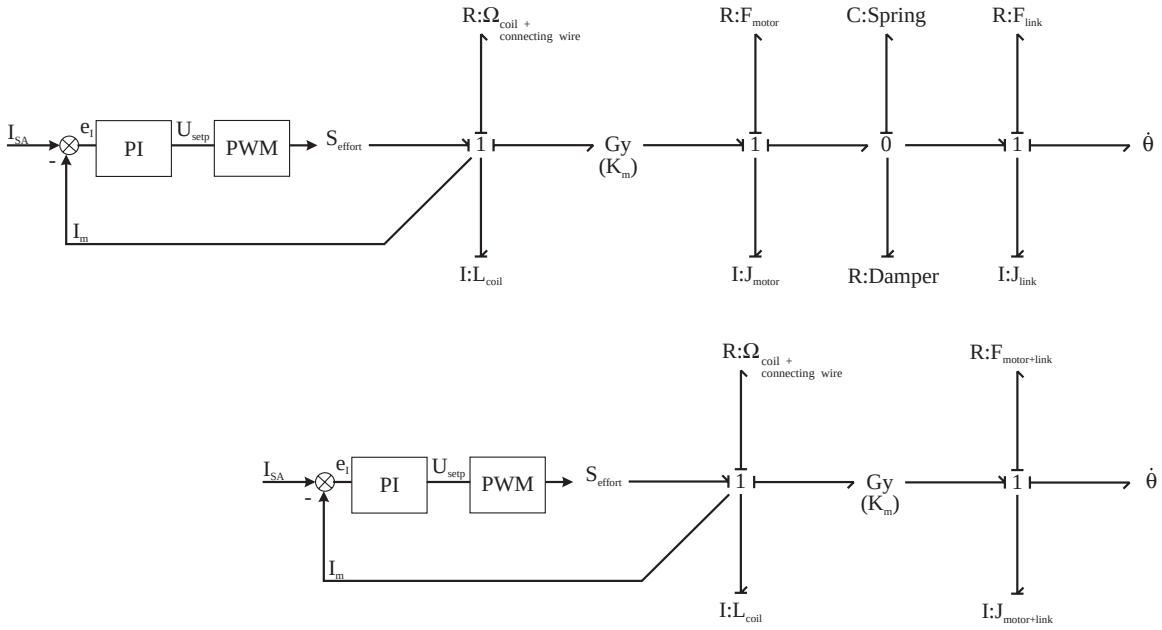

Figure 2.2: *Bondgraph of Servo drive with amplifier.*

The upper graph in figure 2.2 shows the model of the first servo motor, mechanically connected to the first link of the robot. The lower graph shows the model of the second servo motor and link. Several issues on the SCARA control system (servo motor and amplifier with tacho and current feedback) will be discussed in more detail during the explanation of the block diagram, later in this chapter.

Notice that the second joint is considered to be rigid. No spring-damper elements are present between the drive and the link. This is only valid for the second joint because errors are too small to be relevant. This will also be explained later in this chapter.

Sources always fix causality. Since the first junction in the motor is a serial one, all flows have the same value. Suppose we like to impose a current on the serial circuit, because it is proportional to the torque, the cross-stroke must be located opposite to the arrow, since the flow leaves the source.

This causes a problem. To have integral causality on the Inductance, we are contrained to supply a voltage and not a current.

When we draw the diagram, as is done in figure 2.2, and take the above considerations, we see that the causality stroke of the source has to be near the 1-juntion. This automatically implies that a Voltage source has to be used to drive the motor. So, causality of the system demands the input signal to be a voltage. This is a direct consequence of the fact that the armature circuit of the motor has got mostly an inductive nature.

2.3 Modelling the system

In this section we will develop a complete block diagram of the first two axis of the Bosch SCARA system which drives the robot in the horizontal plane. The system consists of the servo motors with gearboxes, the amplifier system and the transputersystem with the user interface.

Step by step the system will be investigated and identified. Parameter values are identified or taken over from data sheets. Deviations from these values in the sense of uncertainties or disturbance will be considered in the next section.

2.3.1 The Servo Motor System

The servo drive can be modelled as a standard DC-motor. It is mechanically connected to the link via a gearbox. The system is activated with a driving Voltage. The output value will be the joint velocity of the corresponding link.

In figure 2.3 the block diagram of the armature controlled DC-motor, derived from the standard servo

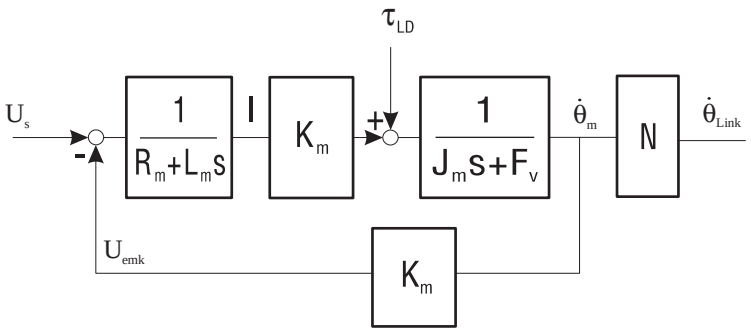

Figure 2.3: *Model of the Servo motor.*

model in [Dor89] on page 52 is reported. Most of the parameters of the motor are specified by the manufacturer. However, some of them are slightly different, for example the resistance turns out to be higher than the value given by the manufacturer. This is caused by the fact that the connecting wires are taken into account and the manufacturer did not do this.

The Laplace form of the transfer function of the servo system is a second order equation in s. It is possible to divide it into two parts. One for the actual undisturbed system and an additional transfer function from the disturbance torque input τ_{LD} to joint velocity $\dot{\theta}_{Link}$.

$$\frac{\dot{\theta}_{Link}}{U_s} = \frac{NK_m}{J_m L_m s^2 + (F_v L_m + R_m J_m)s + F_v R_m + K_m^2} \tag{2.1a}$$

$$\frac{\dot{\theta}_{Link}}{\tau_{LD}} = \frac{NR_m + NL_m s}{J_m L_m s^2 + (F_v L_m + R_m J_m)s + F_v R_m + K_m^2} \tag{2.1b}$$

First we have an inherent emf-feedback loop with amplification K_m, corresponding to the electrical constant of the motor. L_m corresponds to the inductance of the motor coil, R_m is the resistance of the coil plus the connecting wires, F_v stands for the viscous friction and N is the speed reduction of the gearbox. J_m corresponds to the inertia of the motor. For the second link, this inertia includes the reduced inertia of the link of the robot arm.

U_s stands for the voltage input supplied to the motor and $\dot{\theta}_{Link}$ is the resulting joint velocity in radials per second. τ_{LD} is the collection of the perturbing torques (Coulomb friction and stiction etc). Disturbance torques that act on the link are reduced by the factor N and included in τ_{LD}.

Of course an index will be given to the parameters, when the equations involve a servo motor of a particular axis. Table 2.1 shows all the estimated values for the parameters.

Servo/Link 1	value	units
F_{v1}	0.001	$[Nms/rad]$
F_{vL}	90	$[Nms/rad]$
K_{m1}	0.24	$[Nm/A]$
R_{m1}	1.45	$[\Omega]$
J_{m1}	$1.075\ 10^{-2}$	$[kgm^2]$
L_{m1}	$\leq 1.5\ 10^{-3}$	$[H]$
N_1	129^{-1}	[1]
L_1	0.445	$[m]$

Servo/Link 2	value	units
F_{v2}	0.005	$[Nms/rad]$
K_{m2}	0.099	$[Nm/A]$
R_{m2}	1.87	$[\Omega]$
J_2	$4.2\ 10^{-4}$	$[kgm^2]$
L_{m2}	$\leq 1.0\ 10^{-4}$	$[H]$
N_2	101^{-1}	[1]
L_2	0.355	$[m]$

Amplifier 1	value	units
K_{P11}	27.9	[1]
K_{I11}	646.5	$[sec^{-1}]$
τ_1	$8\ 10^{-5}$	$[sec^{-1}]$
K_{P12}	1.42	$[V/A]$
K_{I12}	227	$[V/As]$

Amplifier 2	value	units
K_{P21}	28	[1]
K_{I21}	413.3	$[sec^{-1}]$
τ_2	$8\ 10^{-5}$	$[sec^{-1}]$
K_{P22}	2.67	$[V/A]$
K_{I22}	280	$[V/As]$

Table 2.1: *The various nominal parameter values as estimated.*

2.3.2 The Servo Amplifier System

The manufacturer provides a complete control system to drive the robot. It includes safety and feedback loops, pulse width modulators to drive the servos and setpoint limiters. The safety loops and the setpoint limiters cause no effect in the control system in nominal operation. They act only in excessive circumstances in a way that they bound the performance of the system if we would like to develop a very fast robot controller. Investigation of the effects of these devices are beyond the scope of this report.

The amplifier system contains a current and tacho feedback loop. With these loops both the speed and current tracking are controlled. The tacho loop has the effect of a velocity controller. In the present case, the setpoint represents an angular velocity. This is a problem because it is physically more meaningfull to drive the torque that has to be supplied to the mechanical system. A control signal for the torque could be evaluated and set-pointed to the motor.

Identification of the amplifier subsystem is performed from the circuit diagrams and off-line mearurements. This last method is empirical. This means that a good insight of the characteristics of the system is known at forehand, but that parameters have to be estimated. This estimation is performed with a signal generator and an oscilloscope.

Identifying a system in closed loop is very difficult. Where it is possible, identification of these systems is performed by opening the loop or by disabling the feedback signal in another way. Then the system in open-loop state can be identified straight forward. In this case it is not allowed to leave out the tacho feedback because of a strongly amplifying and integrating error signal. The robot arm would bounce against its bounderies immediately during open-loop measurements. Furthermore, the circuit shows a

second loop, controlling the current of the motor.

Consider that these feedback signals come straight from the motor and are not zero only if the motor is connected (and moving). This means that by disconnecting the motor, the feedback will be disabled. The open-loop system can then be identified off-line. Therefore the printed circuit board (*PCB*) of the amplifier has been pulled out of the rack and connected with an external power supply. With a square wave generator and an oscilloscope the amplifier can be identified. In figure 2.4 parts of the circuit of the amplifier are shown with the particular OpAmps performing the PI-action being drawn bold. Figure 2.6 shows the identified model description in the form of a block diagram of the servo amplifier. It helps to imagine how the identification of the amplifier of the second axis takes place.

The value of the tacho signal is subtracted from the velocity setpoint. This velocity error e_U enters the first PI-controller of the amplifier. In order to identify this PI-controller, R23 is disconnected from the circuit. Now the OpAmp has no Tacko feedback anymore. A square wave is supplied to the open input of the OpAmp where R23 was connected first. The result is measured at point UN (pin 9b of the Optimizing board). Simulations with the identified models of the velocity controllers of both axes show the behaviour in figure 2.5. During measurements also a first order transition effect at the time when the input signal jumps from low to high voltage could be noticed.
This means that the transfer function would look like

$$\frac{I_{sa}(s)}{U_{sa}(s)} = \frac{1}{\tau s + 1}\left(K_{p1} \; + \; K_{i1}\frac{1}{s}\right). \tag{2.2}$$

The first order effect is however not taken into account for the rest of this thesis. This is allowed because the sample time we use in the control environment is 1 msec and the signal is settled at 0.4 milliseconds.
After this first PI-controller, a signal limiter guards the current setpoint I_{sa} for the second PI-controller of the amplifier. The limiter has no effect in normal operation.

The servo motor current flows through a very small well known resistor. The voltage on the resistors is rectified and filtered and gives a steady value of the motor current. This signal is subtracted from the current setpoint of the first PI-controller. The resulting current error e_I is the input signal of the second PI-controller. Notice that the value of the signal represents a current but is in the physical system a voltage signal.

In order to identify this part, R28 is disconnected. A square wave is supplied at pin 9b of the optimizing board. The oscilloscope is connected to pin 4a. Simulations with the identified models of the current controllers of both axes show the behaviour in figure 2.5.

Looking at figure 2.6 the amplifier makes use of a current feedback loop to drive the servo motor. The current PI-controller thus has to transform the current setpoint into a voltage. Notice the units in table 2.1. This voltage is inverted and both the inverted and non-inverted signal are used by the Pulse

Figure 2.4: *Parts of the electrical circuit of the system with the focus OpAmps drawn bold.*

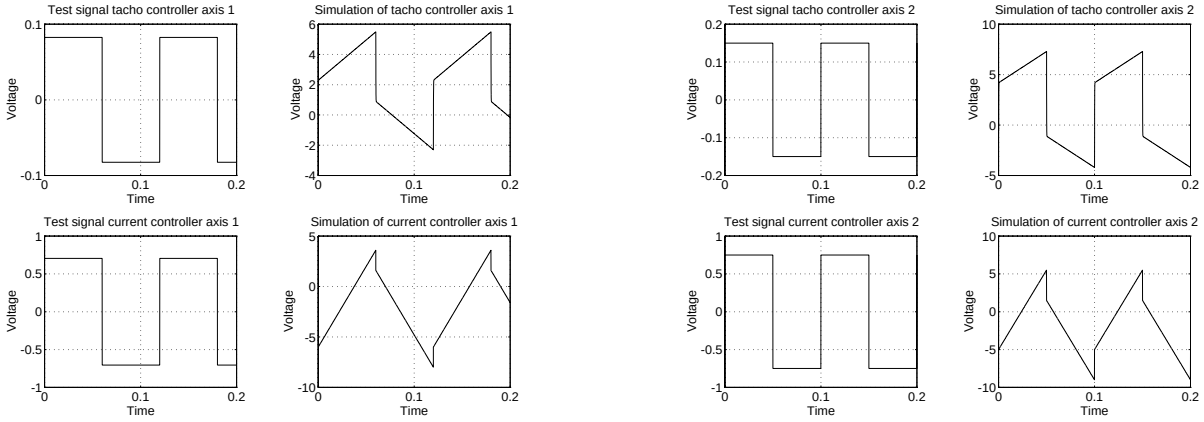

Figure 2.5: *Simulations of the first and second part of the amplifier.*

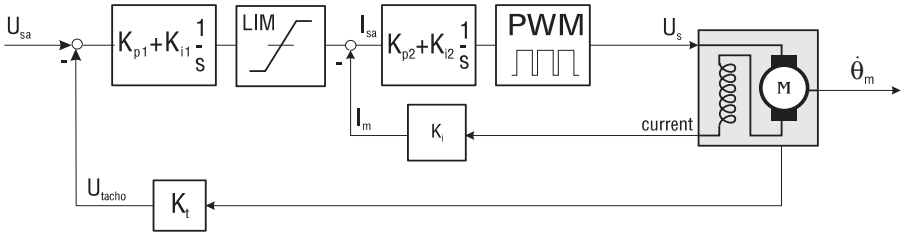

Figure 2.6: *Block diagram of the servo amplifier.*

Width Modulator (*PWM*), which generates the driving signal for the motor. Under normal circumstances, the average output voltage of a PWM is equal to the setpoint. Only when the PWM has to modulate excessive large setpoints, the PWM may show non-linear effects in the average output. These may be caused by the transition effects of the transistors in the PWM when upper or lower pulses become very tight. Because of the presence of large cooling-bodies that have to preserve the four darlington transistors of each motor, transitions may assumed to be not ideal. However it is never possible to drive the PWM with these kind of excessive signals because the limiters of the velocity controller will prevent them from doing so, before they enter the PWM.

It is important to remind that the physical behaviour of a PWM is fully non-linear. The PWM represents actually a bang-bang behaviour. Nevertheless, the average output is the same as the value of the setpoint. Considering low bandwidth for the motor, the PWM can be considered as an amplifier with gain one. The presence of the PWM has a considerable advantage in the energy dissipation of the transistors. This is because the PWM switches between full-current and no current through the transistors, and always when a current flows through the transistors, the voltage on them is zero. In this way hardly any power is dissipated in the transistors.

After the PWM the input voltage is being filtered by a first order system, caused by inductance and the resistance of the motor armature. In Laplace transform it has the transferfunction $\frac{1}{L_m s + R_m}$. The break frequency of the filter is $\omega = \frac{1}{\tau}$ with $\tau = \frac{L_m}{R_m}$ and has a value of at least 2976 Hz for the second axis and at least 1540 Hz for the first axis. Measurements will be done at a sampling rate of 1 kHz. An additional noise input could be modelled just after the PWM. Because the ripple is filtered out for the feedback current signal no effect has been measured from it. The additional noise input will not be incorporated in the model.

The measurement described in this section is also applied on the amplifier of the first axis. The results of the measurement are shown in table 2.1. A presentation of the amplifier system is given in figure 2.6. To verify the estimated parameters, the identified models of the amplifiers are implemented in PSIE. The same test signal as was used for the estimation is supplied to the models to compare the simulation with the real measurement. The ossiloscope displayed the same plots as drawn in figure 2.5.

The model description of the amplifiers in PSIE is included in appendix 7.2

2.3.3 The horizontal plane

The SCARA robot uses the first two joints to move around in the horizontal plane. Only these axes are dynamically coupled. The third and fourth axis can be considered as decoupled mechanically from the motions of the other axes.

The theoretical description of the robot dynamic behaviour can be expressed as a set of closed form

dynamic equations. These dynamic equations express the joint torques as functions of the joint positions, velocities and accelerations.

The general shape of the closed form dynamic equations for all rigid mechanical structures is expressed as:

$$\boldsymbol{M}(\theta)\ddot{\theta} + \boldsymbol{C}(\theta,\dot{\theta}) + \boldsymbol{F}(\theta,\dot{\theta}) + \boldsymbol{G}(\theta) = \boldsymbol{T} \tag{2.3}$$

In equation 2.3 $\boldsymbol{M}(\theta)$ is the inertia matrix, $\boldsymbol{C}(\theta,\dot{\theta})$ is the vector with Coriolis and centrifugal terms and $\boldsymbol{G}(\theta)$ is the gravity vector. The term $\boldsymbol{F}(\theta,\dot{\theta})$ is the component with Coulomb friction, viscous friction and stiction terms.

Complete description of the model, as it is derived applying the Newton-Euler iterations, is found in the Ph.D. theses of de Haas [DH92] and Rieswijk [Rie92].

Since the first two axes only move the robot in the horizontal plane, the Gravity vector $\boldsymbol{G}$ is zero. In this section a brief summary describing the derived model is given. The inertia and Coriolis matrices for the Bosch SCARA follow:

$$\boldsymbol{M}(\theta) = \begin{bmatrix} I_1 + 2I_2\cos(\theta_2) & I_3 + I_2\cos(\theta_2) \\ I_3 + I_2\cos(\theta_2) & I_3 \end{bmatrix} \tag{2.4}$$

$$\boldsymbol{C}(\theta,\dot{\theta}) = \begin{bmatrix} -2I_2\sin(\theta_2)\dot{\theta}_1\dot{\theta}_2 - I_2\sin(\theta_2)\dot{\theta}_2^2 \\ I_2\sin(\theta_2)\dot{\theta}_1^2 \end{bmatrix} \tag{2.5}$$

The values of I_1, I_2 and I_3 depend on the mass distribution in the links, on the link lengths and on the load mass. They are calculated and given by

$$I_1 = 7.46 + m_l(L_1^2 + L_2^2) \tag{2.6}$$

$$I_2 = 1.68 + m_l L_1 L_2 \tag{2.7}$$

$$I_3 = 1.5 + m_l L_2^2 \tag{2.8}$$

The scalars in these equations depend on the structure of the robot. They contain link sizes, positions of centers of masses and masses of the links. The derivation of these terms can be found in [Rie92]. In these equations m_l represents the extra load mass caused by an assembly tool in the gripper of the robot arm, for example. The parameters L_1 and L_2 stand for the geometrical lengths of respectively the first and the second link of the robot arm. They are given in table 2.1.

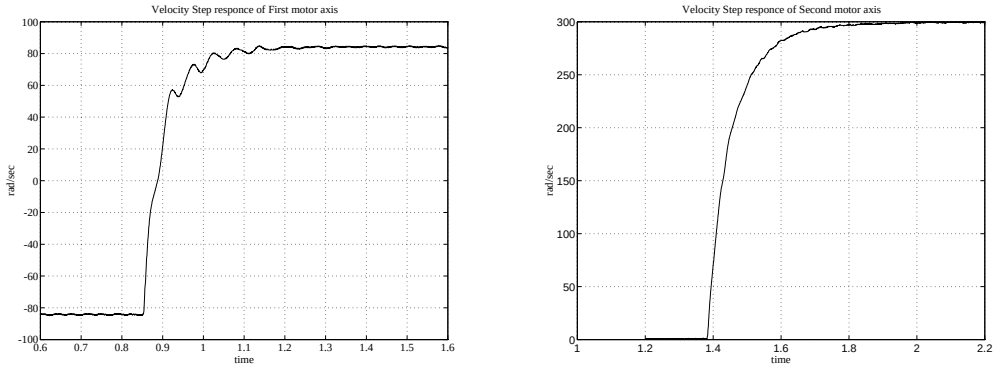

Figure 2.7: *Velocity step responses of the first two axis*

This model does not yet include the actuator dynamics and friction effects. To incorporate these effects into the model, the Newton-Euler equations are combined with the equations describing the DC motors.

From measurements it has been shown that there is an additional effect that has to be incorporated into the model. This is the flexibility of the harmonic drives. Especially the harmonic drive of the first axis has a considerable effect on the dynamic response of the system and thus cannot be ignored.

Figure 2.7 plots the responces of both motos axes for a separate -25/25 Voltage step on the belonging motor. During both measurements the voltage step is only put on the motor that belongs to the motor axis. To avoid direct coupling as much as possible, both links are positioned perpendicular to eachother [Rie92].

Analyses of the step responses shows considerable flexibility of the harmonic drive of joint 1. This flexability will be incorporated in the model as a torsial spring between the motor axis and the joint.

Consider this spring-damper subsystem located between the gearbox and the Link axis. Then suppose the angular difference them is denoted by $\delta_\theta = \theta_m - \theta_L$. This difference is also the result of the integration of the velocity difference. In Laplace this means $\delta_\theta = \frac{1}{s}\delta_{\dot{\theta}} = (\theta_m - \theta_L)\frac{1}{s}$.

Hooke's Law [Roe87] for a spring says that small deviations are proportional to their cause (approximately). This means that $\vec{F}_v = -b\vec{u}$, where b is the spring constant $\vec{F}_v$ the force and $\vec{u}$ the displacement. Furthermore, a linear damper causes a negative acting force proportional to the velocity. Remember that we have the angular velocity between the gearbox and the link and we can calculate the angle by integration, the equation for the spring-damper system in Laplace transform is like

$$\tau_{Link} = K_S\delta_\theta + D_S\frac{\partial\delta_\theta}{\partial t} = K\delta_{\dot{\theta}}\frac{1}{s} + D_S\delta_{\dot{\theta}}. \tag{2.9}$$

Here K_S represents the spring constant and D_S represents the damping constant. With the speed reduction in the gearbox, denoted by N_1, the velocity error becomes $\delta_{\dot{\theta}} = N_1\dot{\theta_{m1}} - \dot{\theta_{L1}}$.

This spring and damper subsystem connects the motor to the link. The difference in the joint positions and velocities produce a driving torque to the link. Since the flexibility effects of the second link are negligible, the gear system of the second axis is considered rigid for the rest of this report. The model is shown in figure 2.8. This simplification introduces a combination of terms in the friction term as follows

$$F_{v2} = F_{vm2} + N_2^2 F_{L2}. \tag{2.10}$$

Here, combined viscous friction F_{v2} consists of the motor friction F_{vm} and of the friction that acts on the second robot link F_{L2}, reduced by the transmission rate N_2 of the gearbox of the second joint. For the first axis two different inertias and viscous friction constants are present. One set of coefficients for the motor subsystem and one set for the link subsystem with the spring-damper subsystem connecting them. The model of the second axis has one combined inertia and one combined friction coefficient. Additional nonlinear disturbance torques like coulomb friction or stiction will be incorporated in the disturbance inputs τ_{LD1} and τ_{LD2}. They will be treated in the next section.

The complete system that takes care of the horizontal movability of the Bosch SCARA robot, is drawn in figure 2.8. It shows the complete control environment of the first two joints.
Clearly for the first axis, the servo motor and the link are dynamically coupled via the spring-damper subsystem. For the second joint, the motor and link systems are wrapped together.

The cross-coupling effects (inertia, coriolis and centrifugal forces) are not drawn completely in the figure but have been grouped together in two blocks. The expressions for the blocks are the elements of the vector $\boldsymbol{C}(\theta, \dot{\theta})$ in equation 2.5.

If an additional load mass is attached to the robot, the inertias will change. In equations 2.11 the relation between additional load mass and the effective inertias are given.

$$J_c = \boldsymbol{M_{1,2}} = 3.18 + m_l L_2^2 + m_l L_1 L_2 \cos(\theta_2) \tag{2.11a}$$

$$J_2 = N_2^2 \boldsymbol{M_{2,2}} + J_{m2} = 4.2\ 10^{-4} + m_l L_2^2 N_2^2 \tag{2.11b}$$

$$J_{L1} = \boldsymbol{M_{1,1}} = 7.46 + m_l(L_1^2 + L_2^2) + 2 m_l L_1 L_2 \cos(\theta_2) \tag{2.11c}$$

Here the M terms stand for the matrix elements of the inertia matrix in equation 2.4. Again the L_1 and L_2 are the lengths of the links, and m_l is the additional load mass. N_2 is the gearbox reduction and θ_2 is the angle position of the second joint. Notice figure 2.9 where the robot arm is seen from above in null-position. So $\theta_1 = 0$ rad and $\theta_2 = 0$ rad.

The cross coupling between link 1 and link 2 is caused by coriolis, inertia and centrifugal forces. From

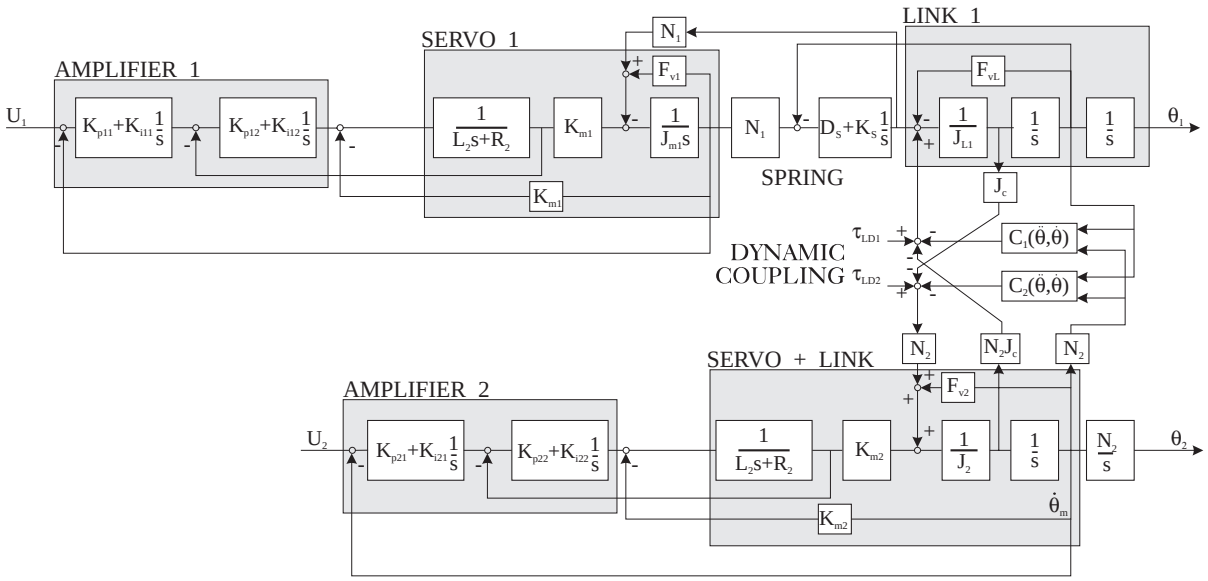

Figure 2.8: *Model of the horizontal movability of the Bosch SCARA.*

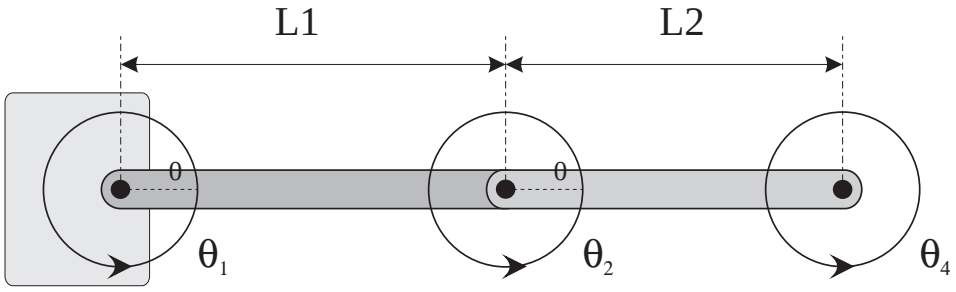

Figure 2.9: *Schematic upper view of the Bosch SCARA in the null position.*

equation 2.11 it can be seen that deviations of the inertias are not only caused by the change of the load mass but also depend on the position of the second joint. The joint position is also of influence on the damping parameter in the spring-damper part of the model. Rieswijk did an empirical parameter optimization of this effect for $m_l = 0$ and $m_l = 4.2$ kilograms [Rie92]. In figure 2.8 the cross-couling terms are not completely geven, but they refer to the coriolis vector in equation 2.5.

Table 2.2 gives the values of the parameters for different joint positions of Link 2. The table shows different values for the spring parameter and damper parameter. This is not obvious and the values at $\theta_2 = 0$ rad will be chosen as the nominal values for the parameters.

In his thesis Rieswijk assumed the dependance of the damping parameter just because simulations gave better results when D_S was to be adapted to θ_2.
A possible explanation could be the fact that the gravitational force causes a longitudinal torque to exist in the first link, if the second link is positioned perpendicular to the first one. This torque could perhaps

Parameter	$\theta_2 = 0$	$\theta_2 = \frac{1}{2}\pi$	$[units]$
J_{L1}	10.9	7.46	$[kgm^2]$
K_S	8.2 10^4	7.6 10^4	$[Nm/rad]$
J_c	3.2	1.5	$[kgm^2]$
D_S	21	23	$[Nm/(rad/s)]$

Table 2.2: *Different values for inertias and the damping for different joint positions of link 2.*

influence the model parameters of the mechanical connection of the first link to the pedestal of the robot. Another explanation could be given, that says that the dependance of the spring-damper parameters is caused by small irregularities of the gearbox. Later on, in this chapter, we will see that also the friction is influenced by irregularities of the gearbox. If the mechanical connection is more tight in certain angular positions than in others, this could cause K_S and D_S to deviate slightly.

No further attention will be given to this effect. The nominal values for the rest of this report will be $K_S = 8.2\ 10^4$ Nm/rad and $D_S = 21$ Nms/rad.

The inertia of the first joint depends on the distance of the first axis to the center of mass of everything that is connected to the first link and that moves when the first servomotor is activated. This means that the distance of the first axis and the center of mass of the second, third and fourth link is of importance for the dynamical behaviour of the first joint. This distance is changed when the second joint is being moved into another joint position. This is the reason why θ_2 in table 2.2 has influence in the inertia of the first axis. The value of the inertia at $\theta_2 = \frac{1}{2}$ rad is however not a true minimum. Obviously, when $\theta_2 = \frac{3}{4}\pi$ rad the center of mass of the second, third and fourth link are even closer to the first axis, so the inertia there will even be smaller.

2.3.4 The Transputer System

In order to control the SCARA, the complete system as being delivered by Bosch has been extended with the transputer system of the control laboratory. This transputer system is connected to the computer network, where SUN workstations are used as the interface between the human operator and the running processes in the transputers.

The transputers have access to the Bosch robot, making use of AD-DA converters. The characteristics of these devices determine the speed and accuracy of the digital control system. They also determine the depth of our investigation because it will not be wise to go into a disturbance deeply, if we know at forehand that the norm of it's maximum effect is less than half the resolution of the conversion devices. The gearbox irregularities, mentioned in section 2.4.3 are too small to be considered. Compare figure 2.12 with the AD-resolution in table 2.3.

Timing considerations, for instance, make it not necessary to take the first order effect of the first part of the servo amplifier into account. See the remark in section 2.3.2 on page 19.

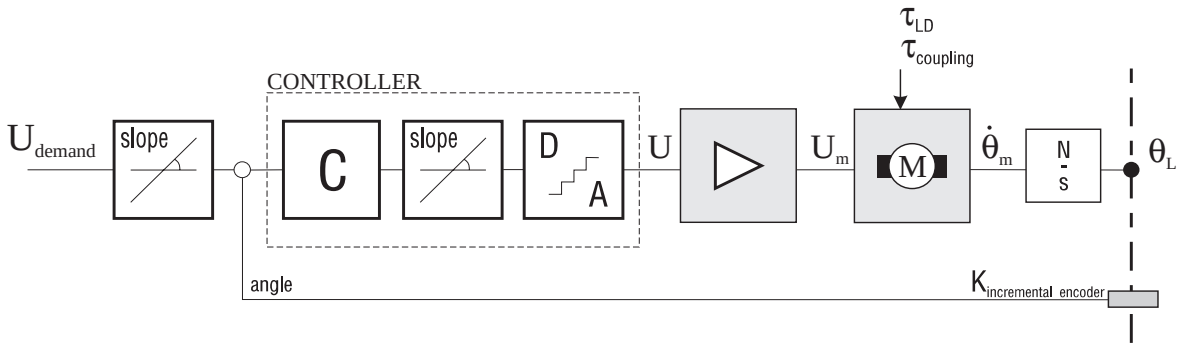

Figure 2.10: *The control environment of one joint from user to link position.*

The control environment for one servo drive is shown in figure 2.10 leaving out cross coupling terms between links. It shows all signal processing by the transputers outside the gray areas. A position setpoint can be supplied by the user interface. An algorithmic slope causes the setpoint not to change too fast. This is necessary because currents could climb too high and cause some safety circuits to trigger in the amplifier system. Then the joint position of the particular joint is read from the incremental encoder and taken into account and a control signal is calculated which should move the arm to the demanded position. Again a slope is inserted to protect the amplifier from excessive velocity setpoints. Finally every one millisecond the prepared value is supplied to the DA converter. The offset of the converter is corrected inside the amplifier.

If the user wants to control the velocity of the robot, a velocity feedback signal is calculated artificially by diffrentiating numerically the values of the incremental enconders. The maximum error on the velocity signals will be twice as large as the maximum error on the joint position signals. Suppose we have two measurements of one joint angle $\theta_1 = \theta_{1r} + \delta_1$ and $\theta_2 = \theta_{2r} + \delta_2$. Here θ_{1r} represents the real joint angle during the first measurement, perturbed with the inaccuracy δ_1. If h is supposed to be the sample time, the velocity is calculated as

$$\dot{\theta} = \frac{\theta_2 - \theta_1}{h} = (\theta_{1r} - \theta_{2r})\frac{1}{h} + (\delta_1 - \delta_2)\frac{1}{h} \tag{2.12}$$

We assume the inaccuracy of any joint angle measurement to be less than the maximum quatization error of the sensor. So $\|\delta_i\| < \delta_{AD}$. For the maximum error in the velocity holds $\|\delta_{\dot{\theta}}\| < \frac{2}{h}\delta_{AD}$.

2.4 Beyond the nominal values

In this section all important deviations of the nominal model will be considered. The aim is to construct separate loops outside the nominal model with all the uncertain and deviating elements of parameters and

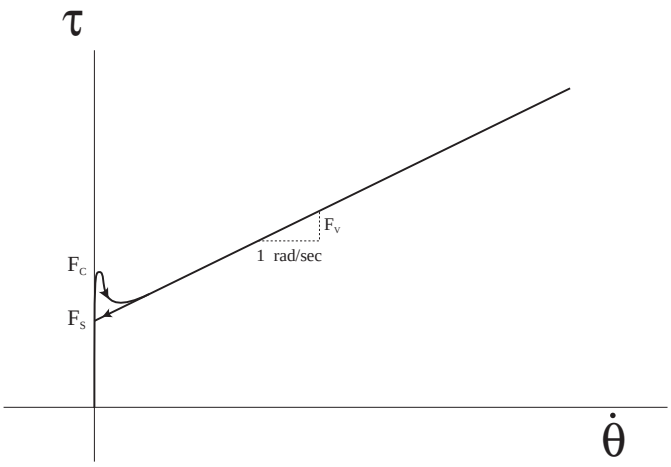

Figure 2.11: *Visualization of different friction effects.*

signals.

The underlying philosophy of the interconnection of the robust control model will be explained in the next chapter. For now we use the model of figure 2.8 and discuss the perturbations and deviations of the system.

I emphasize here that a margin of uncertainty can be created for all parameters. It is however the goal of this report to develop a controller to make the robot drive well under all circumstances. Therefore only relevant differences which influence the behaviour *measurably*, will be treated.

2.4.1 Rigidity

Section 2.3.3 described the dynamic model of the first two joints. Considering rigidity, the first joint connection is modelled as a combination of a spring and a damper because the flexibility is considerable. The possible dependance of the spring-damper parameters was discussed in section 2.3.3.

This is not done for the connection of the second servo motor to the second link, because an error was hardly measurable. No further measurement was done to get an impression of the accurate size of the error, introduced by this neglection. From figure 2.7 it can be seen that identification of this flexability would give unreliable results, that vary from measurements to measurement.

2.4.2 Load mass

Equations 2.11 show that the load mass is a factor in the inertia terms of the two links. It may be obvious that a change of this mass results in a change of dynamical behaviour of the system. The gripping of

different tools for example can be viewed upon as a disturbance of the nominal dynamical characteristics. In this report the maximum allowable load mass will be assummed to be 5 kg.

2.4.3 Disturbance Torques

Reconsider the two inputs τ_{LD1} and τ_{LD2} in the model of figure 2.8. These are collections of disturbance torques of the servo system and of the mechanical system. They consist mainly of the Stiction F_s and Coulomb friction F_c.

These non-linear friction parameters are identified with an analog current source, which we use to drive the motor. The static friction can be determined by slowly increasing the current until the motor starts to rotate. The current I_m that is present just before the motor starts turning corresponds to the Stiction. The stiction is correlated to I_m, according to

$$F_S = K_m I_m \tag{2.13}$$

with K_m being the motor constant. Once the motor is turning the current is slowly decreased until the motor stops again. This current corresponds to the Coulomb friction. Table 2.3 shows the estimates of the friction parameters. Figure 2.1 shows an open-loop ramp responce of the second joint. It should be mentioned that this is a good method for the general case, if F_C and F_S are not dependant on θ. However, figure 2.12 shows that friction depends on the angular position of the motor axis.

One of the aspects that greatly influences the measurements is the initial motor position. The motor axis or a part of the gearing that is rotating at the same speed as the motor axis, does not turn completely smoothly. A velocity measurement of the fourth joint in figure 2.12 shows this effect clearly. The period of the motor axis revolution can be determined form the average link velocity. This period (0.25 sec) is the same as the cycle time of the periodic change in the link velocity. It shows that at certain angular positions the friction is less than at others. This causes the stiction to be dependent on the initial motor position. The estimates of the stiction and Coulomb friction are shown in table 2.3. They are taken from [Rie92].

From these measurements it can be concluded that the friction cannot be described using two constant torques for the Coulomb friction and the stiction.

These friction effects are graphically explained in figure 2.11. It shows that there must be a certain minimum torque for all $\dot{\theta} > 0$. Coulomb friction and Stiction cause the non-linear effect near $\dot{\theta} = 0$. The third friction effect is linear dependant on the angular velocity $\dot{\theta}$. It is called the viscous friction.

Because all of these friction effects are not easy to determine (uncertainty) and vary from measurement to measurement (perturbations), the values for the parameters are split in a nominal part and an additional

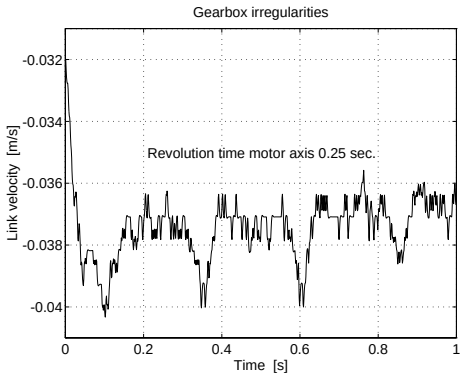

Figure 2.12: *Velocity variations, due to gearbox irregularities of the third joint.*

Torque	joint 1	joint 2
$F_s[Nm]$	17.92	11
$F_c[Nm]$	14.1	9

AD-DA accuracy
δ_{AD1} = 2.3 10^{-2} $[rad]$
δ_{AD2} = 2.9 10^{-2} $[rad]$
δ_{DA} = 2.5 10^{-3} $[Volt]$
h = 1 10^{-3} $[s]$

Table 2.3: *Estimated parameter values for Stiction and Coulomb Friction and the accuracy of the IO-facilities of the transputer system.*

disturbance part. We take a safe margin of $\pm$10% uncertainty on the viscous friction parameters. With these friction models we proceed in this report to find a robust controller.

2.4.4 Interaction between the two joints

In figure 2.8 it can be seen that there is interaction between the two joint systems. The interaction appears in the joint systems as torques on the joint axes. section 2.3.3 is referred to for the discussion on the interaction. Table 2.2 shows the dependance of certain parameters of the first joint system on the joint position of the second axis. Equations 2.11 again show the dependance.

Because it is in the focus of this report to develop two independant controllers, this interaction will be seen as independant disturbance torques. It may be clear that this way of not using important knowledge of the system for the design of the controller results in a conservative control law. In this report, this is mostly done for a didactical purpose. In the recommandations this will be discussed again.

In figure 2.8 it can be seen that the cross-coupling is caused by the coriolis terms, given in equation 2.5. From that equation it can be seen that interaction depends among other states, on the angular velocity $\dot{\theta}$ of the other joint. In chapter 4 the maximum possible interaction between the joints has to be estimated. Therefore boundaries have to be posed for the velocities. Here we assume $\dot{\theta}_1 \leq 1$ rad/sec^2 and $\dot{\theta}_2 \leq 1.5$ rad/sec^2. Of course, if these values cause no problems for the stability, more performance can be gained

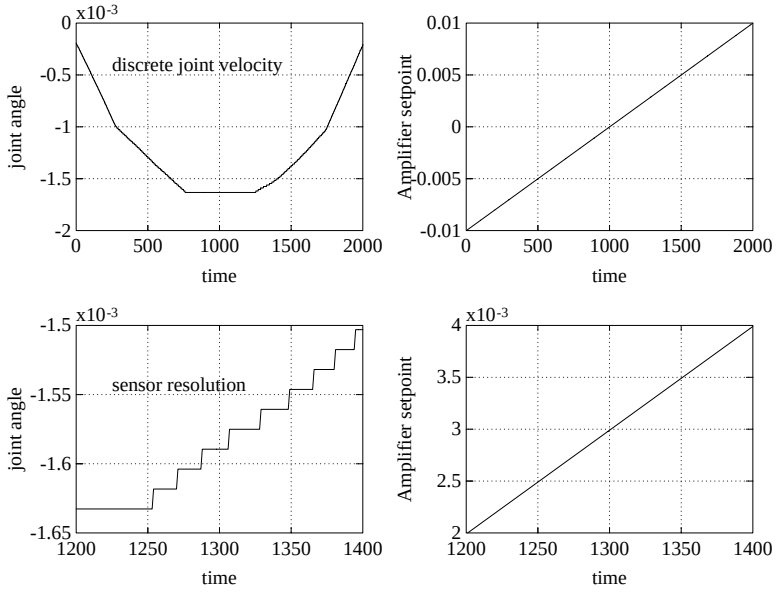

Figure 2.13: *Resolution measurement of the A/D and D/A converters.*

by allowing larger values for the velocities.

2.4.5 AD-DA Conversion

Analog to digital conversion rounds off analogous values to discrete values, presentable by bit patterns. Information between two succeeding presentable values in the analogous signal is lost, converting it to digital numbers. The loss of information is called *Quantisation error*.

Also conversion from binary numbers to analog signals has a limit in accuracy. If ever the operator or the controlling process would like to send a very exact signal to the system and it must be converted from a digital to a analogous representation, the number is bluntly rounded off. The size of this error however is very small and it is in practice almost never a problem.

A measurement can show the effect of the conversion well. In figure 2.13 it can be seen that for a smooth setpoint (upper-right) the arm is controlled stepwise (upper-left). This shows the resolution of the DA-converter. The same setpoint, now zoomed (lower-right) shows again the reaction when the setpoint crosses the half- resolution-value and shows the step-by-step sensor value of the incremental encoder.

In table 2.3 quantization errors are summed up. Both encoders generate 4320 pulses per motor axis cycle. This means an accuracy of 1548 and 1212 pulses per degree of rotation of respectively joint 1 and 2. This means that 1 bit corresponds to 2.3 10^{-2} rad for joint 1 and of 2.9 10^{-2} rad for joint 2.

Finally the communication with the transputer system automatically means that the controllable bandwith

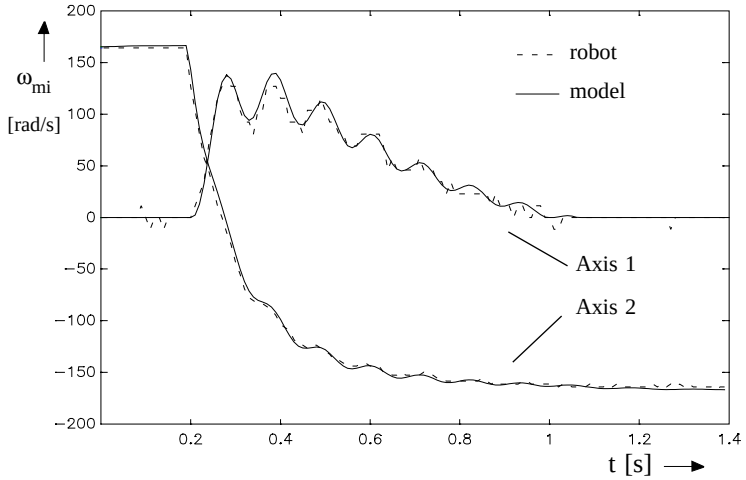

Figure 2.14: *Measured and predicted responce for $\dot{\theta}_{m2}$ to a voltage step of -25/25 Volt.*

is finite and bounded by the sampling time. According to Shannon's Sampling theorem, [Sha49], we may state the following. Allowing no frequecies higher than $\frac{1}{2h}$ Hz on the system, where h is the sampling time in seconds, the AD and DA converters are able to measure and reproduce all signals well without loss of information.

2.4.6 Joint Acceleration

Classical mechanical laws state that the acceleration of an object with a certain mass is proportional to all forces acting on it. Of course when the second joint is addressed with a torque of the motor, it is supposed to gain velocity in a certain direction.

The change of velocity is called the acceleration of the joint and denoted by $\ddot{\theta}_1$. The acceleration on it's turn causes a torque with opposite sign on the first link. The first joint angle is influenced by the torque. Figure 2.14 shows the effect, simulated and measured for a step of the second axis [Rie92].

To estimate the behaviour of the robot arm when two separate joint models are used, constraints have to be posed for the maximum acceleration of the joint axes. For this report they will be $\ddot{\theta}_{1,2} \leq 10$ rad/sec^2.

2.5 Verification of the Identified Model

The preceding sections were intended to clarify how the system is built up. In this section the models ere verified with the real system.

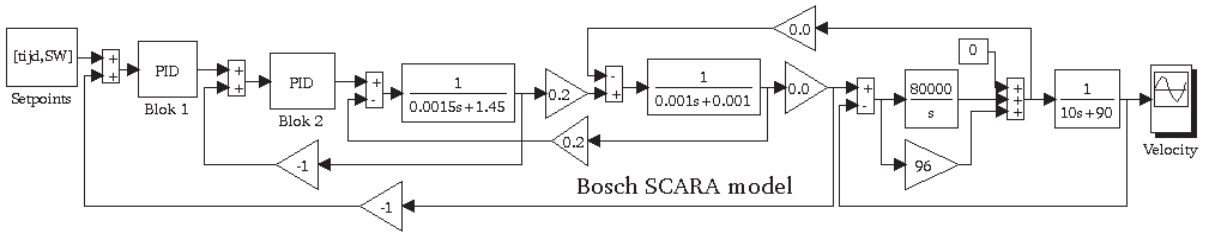

Figure 2.15: *Velocity control model of the first joint, built in Simulink*

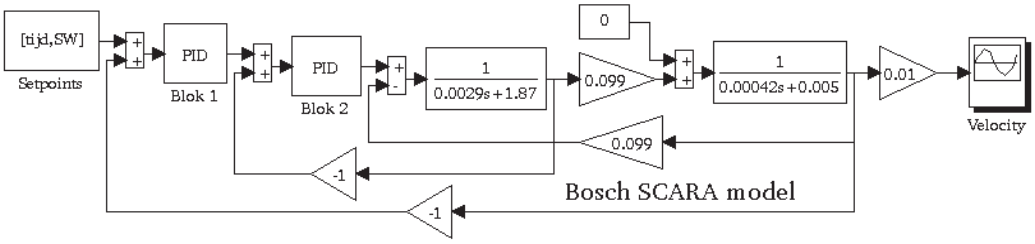

Figure 2.16: *Velocity control model of the second joint, built in Simulink*

For that purpose the joint models are implemented in SIMULINK and a simulation of the system, using the model, will give an impression on its reliability.

2.5.1 Simulation and Verification

The models that are developed in this chapter describe the transfer of commanding signals from the transputer system to the resulting joint positions. That these models are valid and that they describe the real system well, can be verified with a simulation of a step responce.

In order to do so, the model is implemented in Simulink, the simulation toolbox that is part of the Matlab mathematical software packet. Figures 2.15 and 2.16 show these models.

The step responce simulations of the PI-controllers in the model of the servo amplifier were already shown if figure 2.5. The figure shows plots that are equal to the responces on the oscilloscope. The parameters of the PI-models were derived from the plots of the oscilloscope.

Figure 2.7 shows the measurement of a -25/25 Volt step responce directly on the motor armature. This measurement has been simulated with the simulink models. The results are plotted in figure 2.17

The remaining differences are caused by the fact that two separate models for the horizontal movements are used, whereas the first joint is influenced greatly by the movements of the second. This will be discussed in the conclusions again.

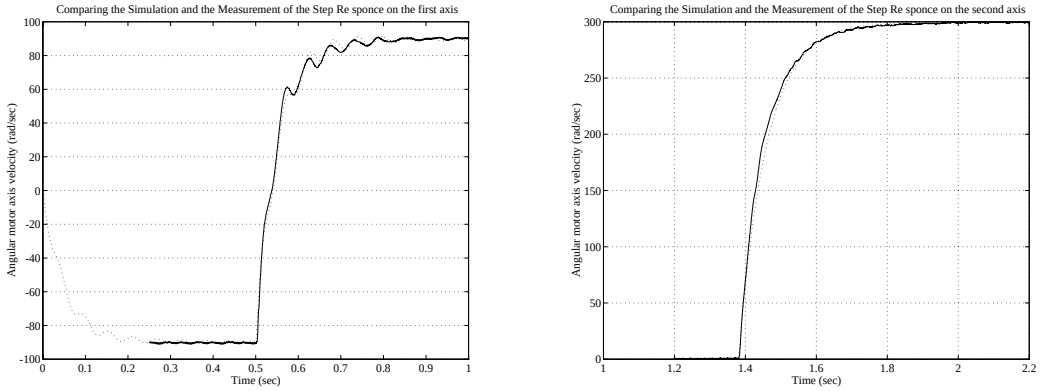

Figure 2.17: *A simulation and a Measurement of a stepresponces of the first two joints of the Bosch SCARA.*

Chapter 3

Robustness in Stability and Performance

In this chapter we take a closer look at the theoretical background of Robust Control. With this background we will be able to construct the model of the Bosch SCARA in the focus of the design of the robust controller. The control problem on the Bosch will be analysed in the next chapter again.

In this chapter a general perturbed system and an example system are presented for a case study. The transferfunction is discussed and we take a look at the *well posedness* and at the *complex structured singular value.*

Further on, control design terms as *stability* and *performance* are discussed in the focus of the robustness of the closed-loop system. This is done for the SISO example system first. Then the resulting definitions are generalized for MIMO systems. An extensive explanation on the H_∞ problem can be found on page 270 of [Mac91]. Most of the explanation given here, has been taken from [DCIoTtT92] and [Smi94].

One way to describe the performance of a control system is in terms of the size of certain signals of interest. Because in the case of the Bosch SCARA, we want the tracking to be as good as possible, we can specify a maximum error on this signal. Some definitions have to be posed to define a signal's size.

3.1 General perturbed system

A general system has several inputs and several outputs. It is called a Multi - Input - Multi - Output (*MIMO*) system. Outputs can be anything like flow, temperature or some position. In the case of the SCARA robot, it will represent the angular velocity of the joint. The outputs depend usually on the characteristics of the system and on the independent input signals like, in the frequency domain,

$$\boldsymbol{y}(j\omega) = \boldsymbol{P}(\boldsymbol{d}(j\omega)) \tag{3.1}$$

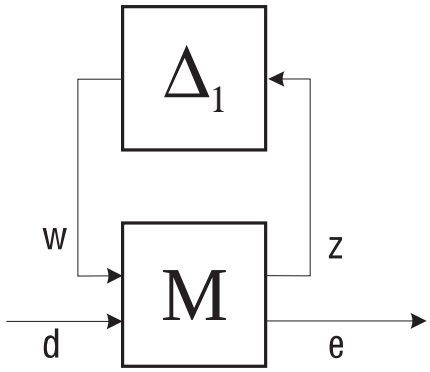

Figure 3.1: *General Closed-Loop Perturbed System Separated in a Nominal and Perturbation part*

where y is the output signals, P is an operator, representing the *MIMO* system and d stands for the input signals.

In real life, systems are hardly ideal. They often suffer from disturbances and more often parts of the system are unknown or uncertain. Chapter 2 considered some disturbances of the SCARA. Perturbations often depend on the state in which the system is. However this is not necessary.

Disturbances can be modelled as sources (independant disturbances) or as transferfunctions (dependant perturbations).
The independant disturbances can be seen as an extra input on the complete system. Equation 2.1 showed the output signal $\dot{\theta}_{Link}$ to be dependent on the setpoint and on an extra independent disturbance torque input.
The dependent disturbances are perturbations or uncertainties of parameters. An example of this kind of perturbation can be seen in equation 2.11c where the load mass m_l perturbes the inertia parameter of the second link. In this case the nominal unperturbed parameter is incorporated in the nominal transfer matrix and an additional perturbation block is positioned parallel to the nominal parameter. The perturbation block is then considered separately from the nominal transfermatrix. This causes the matrix to be expanded with an extra input and output, solely for this perturbation.
Another kind of dependant perturbation is the multiplicative perturbation which will be discussed in the example at the end of this section.

The above described set-up results in a realistic general perturbed system like the one in the diagram of figure 3.1.

Here Δ_1 is the collection of parameter uncertainties and perturbations. The independant disturbances are modelled as input signals. Together with the actual setpoint of the system they are incorporated in d. M is the transfer matrix that includes all well-known parts of the system. e is the tracking error. w and z are respectively the extra inputs and outputs of the transfer matrix to pull out the parameter perturbations.
According to figure 3.1, M can be structured as

$$M = \begin{pmatrix} M_{11} & M_{12} \\ M_{21} & M_{22} \end{pmatrix}, \tag{3.2}$$

In this case, M_{12} has to have the same dimensions as Δ_1. If $\mathbf{\Delta_1}$ stands for the total collection of possible perturbations and disturbances of the system, then for $\Delta_1 \in \mathbf{\Delta_1}$, the system of figure 3.1 and the transferfunction M in equation 3.2 can be described by

$$\begin{aligned} z &= M_{11}w + M_{12}d \\ e &= M_{21}w + M_{22}d \\ w &= \Delta_1 z \end{aligned} \tag{3.3}$$

For design purposes, we are interested in the tracking error of the perturbed system. From the above equations a transfer function can be derived that gives the output error e for example the tracking error) as function of the input d. Some substututions will lead to

$$F_u(M, \Delta_1) = M_{22} + M_{21}\Delta_1(I - M_{11}\Delta_1)^{-1}M_{12}. \tag{3.4}$$

This equation is only valid if for any vector d, there exist unique vectors w, z and e satisfying the loop equations 3.3. If they exist, the set 3.3 is called *well-posed.*

Linear Fractional Transformation It is now easy to see that equations 3.3 are well posed if and only if the inverse of $(I - M_{11}\Delta_1)$ exists. If it does then $e = F_u(M, \Delta_1)d$ is called the Linear Fractional Transformation (LFT) on M by Δ_1.

The problem in designing the controller, focused on the open-loop interconnection matrix consists of two constraints:

DESIGN PROBLEM
- Determine whether the loop equations 3.3 are *well posed* for all $\Delta_1 \in \mathbf{\Delta_1}$, and
- if so then determine how "large" $F(M, \Delta_1)$ can get for this norm bounded set of perturbations.

Take the general closed loop feedback structure like in figure 3.2. We have an arbitrary nominal system that is perturbed according to

$$P_{real} = (1 + \Delta_1)P_{nom} \tag{3.5}$$

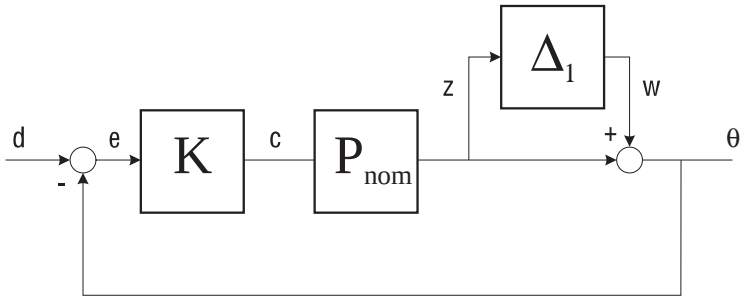

Figure 3.2: A General Closed loop Perturbed System with Controller and Disturbances.

The transfer function P_{nom} in the figure represents the nominal model of the open-loop system and P_{real} the true perturbed system. The transfer function K represents the controller. The Δ_1-block represents the error on the system.
Considering the signals, d is the disturbance or command input, e is the tracking error, c is the control or command signal to the open-loop system and θ stands for the desired output of the closed-loop system. Usually the system output is of no importance in designing a controller. The focus is more on the error signal in the search for maximum performance.

The perturbations are unknown and covered in the Δ_1-block. The rest of the system is assumed to be well known, linear and time-invariant.

Because the controller K is designed explicitly and is therefore well known, it belongs to the nominal part of the system. The interconnection matrix M contains the coefficients to describe the transfer fuctions. Equations 3.3 apply on this system. Notice that the output is of no importance in the design problem and is therefore not produced by M. The symbols in figure 3.2 coincide with those in figure 3.1. Here Δ_1 is a multiplicative disturbance function and it's output is therefore dependant on the output of the nominal system. The input d can of course contain some noise or other disturbance besides the command signal. If the transferfunctions from w and d to z and e are worked out then, with equation 3.3, M becomes

$$M = \begin{pmatrix} -\frac{P_{nom}K}{1+P_{nom}K} & \frac{P_{nom}K}{1+P_{nom}K} \\ -\frac{1}{1+P_{nom}K} & \frac{1}{1+P_{nom}K} \end{pmatrix} \tag{3.6}$$

3.2 Issues on Robustness

If a system is Robust, it performs it's task according to the performance specification under all possible perturbations. The performance specification applies on stability and the accuracy of the tracking of the controlling signal. The latter property can still mean anything and it differs for different kinds of systems. It can for example be a time or frequency function.

To be able to measuere the size of a signal, or the maximum gain in a matrix, a subsection is devoted to norm definitions.

Before we start the complete discussion on Robustness we need some additions on the LFT. They are a deeper mathematical insight on the well posedness of the LFT that was already mentioned. This section will be concerned with this explanation.

In the linear algebra several tools are developed to be able to analyse certain characteristics of matrices. In designing the controller, we want to be able to say something about the maximum amplification of the system's transfer function. For this we can make use of the singular value decomposition *SVD* of the transfer matrix. Therefore a brief mathematical explanation on this, in this section. The explanation will make use of a norm of the transfer matrix. Two important norms will be discussed.

Finally more mathematical insight is given in the Design Problem definition of the preceding section. It concerns the stability and performance of a perturbed system.

3.2.1 Norms for Signals and Systems

Suppose u is the current through a 1-Ω resistor. Then the instantaneous power equals $u(t)^2$. The total *energy* of u is calculated with the integral over time of the power and is equal to the square of the 2-norm. So

$$\|u\|_2^2 := \int_{-\infty}^{\infty} u(t)^2 dt. \tag{3.7}$$

The 2-norm of a signal is *isomorph* in time and frequency which means that it can also be calculated by integrating the square of the fourier transform. This is Parceval's theorem [RC94]. The *average power* of a signal can be related to the *Root Mean Square norm* (RMS)

$$\|u\|_{RMS}^2 = \lim_{T\to\infty} \frac{1}{2T} \int_{-T}^{T} u(t)^2 dt. \tag{3.8}$$

It may be obvious that in an infenitely large interval of time, $\|u\|_2 < \infty$ if and only if the RMS-norm is zero.

To get an idea of the largest occurring value of a signal, we can make use of the ∞-norm. It is defined as

$$\|u\|_\infty := \sup_t |u(t)|. \tag{3.9}$$

For system transfer functions we can define some norms on the amplification. We consider systems that are linear, time-invariant, causal and finite dimensional. In the time domain an input-output model for such a system has the form of equation 3.1. The maximum gain of the RMS-value of the input signal by the system is called the H_∞ norm. So for the system P this means

$$\|P\|_\infty = \sup_{u \neq 0} \frac{\|P(u)\|_2}{\|u\|_2} = \sup_{\|u\|_2 = 1} \|P(u)\|_2 \tag{3.10}$$

A detailed explanation on the operator norms $\|P\|_2$ and $\|P\|_\infty$ can be found on page 99 of [Mac91].

3.2.2 Complex Structured Singular Value

For the multivariable systems there is an extra problem of interactions. To be able to discuss "directional gains" for multivariable systems, one can use singular values.

Take a look at the general feedback scheme in the right diagram of figure 3.1 again. If we consider the internal closed perturbation loop and hold the input d at zero, then the system can be described by the loop equations

$$\begin{aligned} w &= \Delta_1 z \\ z &= M_{11} w \end{aligned} \tag{3.11}$$

Bare in mind that we assume multivariable perturbations. That means that Δ_1 can be a matrix of separate structured complex perturbations or submatrices of perturbations. We assume the perturbation matrix to be like

$$\Delta_1 = \{\text{diag}[\delta_1, ..., \delta_n] : \delta_i \in C\}. \tag{3.12}$$

We will be interested in the gain of the matrices Δ_1 and M_{11} later on in this chapter.

If Δ_1 is structured, it is not hard to find out what the norm of the matrix is. However, with an unstructured matrix like M this is much harder.

Actually the ∞-norm of M is the square root of the largest eigenvalue of $M^T M$: $\|M\|_\infty^2 = \lambda_{\max}(M^T M)$. In case M is symmetric, then $M^T M = M^2$ and the norm is the largest eigenvalue: $\|M\| = \max|\lambda_1|$. In every case, the vector that is amplified the most is the corresponding eigenvector of $M^T M$:

$$\frac{\|Out\|^2}{\|In\|^2} = \frac{x^T M^T M x}{x^T x} = \frac{x^T(\lambda_{max} x)}{x^T x} = \lambda_{max} = \|M\|_\infty^2 \tag{3.13}$$

Forming $M^T M$ can however be a complicated problem. Therefore we can make use of the singular value decomposition $M = Q_1 \sum Q_2^T$. The entries σ_i in the diagonal matrix $\sum$ are the *singular values* of M and their squares are the eigenvalues of $M^T M$. Therefore another formula for the norm is $\|M\|_\infty = \sigma_{\max}$. The matrices Q_1 and Q_2 are ortogonal and therefore leave lengths unchanged in $\|M\|_\infty = \|Q_1 \sum Q_2^T x\|_\infty$, so the largest amplification factor is $\sigma_{\max}$.[Str88]

A special property of $\sigma_{\max}$, if it equals $\|M\|_\infty$ was discussed in the previous subsection. It says that the largest singular value equals the maximum RMS-gain of the input signal,

$$\sigma_{\max}(M) = \max \frac{\|Mu\|_2}{\|u\|_2} \tag{3.14}$$

More on this can be found in [RC94]

Now recapture the stability problem of the LFT. The loopgain of $M_{11}\Delta_1$ has to be smaller than 1. The following definition applies the singular value decomposition on our stability problem.

In our application, the complex structured singular value, which will be indicated with $\mu_{\Delta_1}(M_{11})$, is a measure of the smallest Δ_1, using the defined norm, that causes "instability" of the $M_{11}\Delta_1$ closed-loop.

Now we can take a look at the mathematical formulation of the structured singular value.

$$\mu_{\Delta_1}(M_{11}) := \frac{1}{\min\{\sigma_{\max}(\Delta_1) : \Delta_1 \in \mathbf{\Delta_1}, \det(I - M_{11}\Delta_1) = 0\}} \tag{3.15}$$

It calculates the smallest of all maximum singular values of all possible Δ_1's, which make the system "unstable".
In other words: *When we would slowly increase the size of the perturbations on the system, $\mu_{\Delta_1}(M_{11})$ tells us when the system becomes unstable.* With this proposition the first part of the design problem can be solved.

It may be clear that the singular value of a frequency dependant transfer function will also be a function of the frequency. To trace the maximum singular value in the bandwidth of the transfer function M_{11}, the H_∞ calculation is extended with

$$\|M\|_\infty = \max_\omega \sigma_{\max}(M(j\omega)). \tag{3.16}$$

A deeper insight is

3.3 Robustness in Stability and Performance

In this section the Robust Control theory will be explained by focussing on the SISO example in the beginning of this chapter (see figure 3.2). Robust Control theory involves three main issues :

1. Nominal Performance. What are the system's characteristics if no perturbations are present?
2. Robust Stability. Remains the system internal stability in all possible perturbed situations?
3. Robust Performance. How well behaves the system in the presence of perturbations. Or, how much performace can we guarantee in worst case perturbing situations?

Step by step these issues will be discussed.

3.3.1 Nominal Performance

To be able to tell something on the performance of a system under perturbation, the systems characteristics in the absence of perturbations should be investigated first. This subsection is devoted to that problem.

Important to remind is that the focus of performance in the case of the tracking problem on the Bosch SCARA is the tracking error e. This was mentioned before in the first section of this chapter. If perturbations are supposed zero ($\Delta_1 = 0$), then the transfer function from setpoint to tracking error in the example of figure 3.2 becomes

$$e = \frac{1}{1 + P_{nom}K} d. \tag{3.17}$$

$\frac{1}{1 + P_{nom}K}$ is often referred to as the Sensitivity function, denoted by S.

Always, if a performance specification is supplied with a certain system, it states that the system error has a value of: "at most some value". For the tracking error in the focus of this report, we need a maximum, allowed value for the error in order to be able to say something about the performance.

In the previous section the maximum size of a signal was defined as the ∞-norm. Considering the general frequency dependant transfer function, this means that if we want the error to remain below some β over all frequencies, then this means that for a normed input signal $\|d\|_\infty = 1$, we want

$$\|S(j\omega)\|_\infty < \beta. \tag{3.18}$$

Consider the characteristic of the ∞-norm in equation 3.10 that states that the ∞-norm equals the RMS-gain of the system. So the maximum size of the output signal, if for the input holds $\|d\|_\infty \leq 1$, is: $\|e\|_\infty \leq \|S\|_\infty < \beta$.

Assume a frequency independant situation and a weighting function for the tracking error as

$$W_P = \frac{1}{\beta}. \tag{3.19}$$

Then we know that $\|W_P S\|_\infty < 1$ should hold for all $\omega \in I\!R$ in order to achiev the performance specification If we want the performance to be good for a certain bandwidth, the performance specification can be fequency dependant. This means that for the sensitivity function

$$\|W_P(j\omega)S(j\omega)\|_\infty < 1 \qquad \forall \quad \omega \in I\!R. \tag{3.20}$$

If this inequality holds, than we know for sure that the tracking error will never exceed $\beta(\omega)$.

3.3.2 Robust Stability

In section 3.2.2 the internal stability of the system was allready discussed briefly. In this section the internal stability under perturbations will be given some more attention. Assume all input, output and transfer functions to be frequency dependant and valid for $\omega \in I\!R$. As we are only interested in the internal stability, the input d will be kept zero and the focus will be on the output z.

Again, we refer to figure 3.2 in the example of the first section. Because we will keep d zero and focus on the disturbance loop only, z can be expressed as a function of just w and the transfer function from w to z through the system is then as

$$z = \frac{P_{nom}K}{(1 - P_{nom}K)}w \tag{3.21}$$

This transferfunction is often referred to as the *Complementary Sensitivity function* T, because $T = 1 - S$ holds. Here S represents the sensitivity function that was introduced in the previous subsection. So $z = Tw$ holds.

Nothing is known about the perturbations in Δ_1 except for it's ∞-norm being bounded by some $\beta > 0$. So, for some β, we know in this case that $\|\Delta_1\|_\infty \leq \beta$. Suppose we define a weighting function W_Δ in order to norm Δ_1. This will mean that

$$W_\Delta = \beta \qquad \Rightarrow \qquad \|W_\Delta \Delta_1\|_\infty \leq \beta. \tag{3.22}$$

Assume that $T(j\omega)$ is stable, and that $\Delta_1(j\omega)$ is stable and normed by W_Δ. The internal perturbation loop through $W_\Delta\Delta_1$ and the rest of the system, denoted by T is well-posed and internally stable for all possible perturbations with $\|\Delta_1\|_\infty \leq 1$, if and only if

$$\|TW_\Delta\Delta_1\|_\infty \leq \|TW_\Delta\|_\infty < 1. \tag{3.23}$$

According to the multivariable Nyquist criterion [Dor89] and using the definition of the singular value from section 3.2.2 the loop is internally stable if and only if the Nyquist plot of $\det(I - T(j\omega)(\gamma\Delta_1(j\omega))$ does not pass through, or encircle the origin. If $\|T\|_\infty \leq \beta$ this guarantees for all perturbations with $\|\Delta_1\|_\infty < \frac{1}{\beta}$, any $\omega \in I\!R$ and any scaling $\gamma \in [0, 1]$, the determinant

$$\det\left[I - T(j\omega)\gamma\Delta_1(j\omega)\right] \neq 0. \tag{3.24}$$

This guarantees that the Nyquist plot of $\det(I)$ (if $\gamma = 0$) encircles the origin as many times as $\det(I - T(j\omega)\gamma\Delta_1(j\omega))$ (if $\gamma = 1$). Because $\det(I)$ is just a single point in 1, it does not encircle the origin. Therefore also $\det(I - T(j\omega)\gamma\Delta_1(j\omega))$ does not, and thus stability is proven for $\|T\|_\infty \leq \beta$.

Applying this on the example, we can substitute the transfer function in equation 3.21, which we called the transfer function T, this brings us to

$$\left\| W_\Delta \frac{P_{nom}K}{1 + P_{nom}K} \right\|_\infty < 1. \tag{3.25}$$

It is possible to transform this equation in

$$\|W_\Delta\|_\infty \frac{\|P_{nom}K\|_\infty}{\|1 + P_{nom}K\|_\infty} < 1 \quad \Rightarrow \quad \|W_\Delta\|_\infty \|P_{nom}K\|_\infty < \|1 + P_{nom}K\|_\infty. \tag{3.26}$$

Recall that W_Δ is the function to norm the perturbations and therefore holds the maximum bound on them. So the maximum deviation from the nominal model is W_Δ. Now recall equation 3.5. Implementing the maximum bound on the error, we can write $\|P_{real}K\|_\infty = \|(1 + W_\Delta)P_{nom}K\|_\infty$ with $P_{real}K$ being the open-loop perturbed system. This can be rewritten like

$$\|P_{real}K\|_\infty = \|P_{nom}K + W_\Delta P_{nom}K\|_\infty \leq \|P_{nom}K\|_\infty + \|W_\Delta\|_\infty \|P_{nom}K\|_\infty \tag{3.27}$$

and therefore,

$$\|W_\Delta\|_\infty \geq \frac{\|P_{real}K\|_\infty - \|P_{nom}K\|_\infty}{\|P_{nom}K\|_\infty}. \tag{3.28}$$

Finally, substituting this result in (3.26) gives us

$$\|P_{real}K\|_\infty - \|P_{nom}K\|_\infty < \|1 + P_{nom}K\|_\infty. \tag{3.29}$$

The interpretation of this is that the nominal open-loop system will allways be further away from the critical point -1 than from the perturbed open-loop system. This hereby guarantees robust stability. No perturbation will bring the nominal system onto or beyond the critical point in the Nyquist plot.

3.3.3 Robust Performance

Robust performance means that the closed-loop system is able to track the input signal well, under all possible perturbations, and likewize to keep e small. When analysing the robust performance the terms "well" and "small" have to be defined first. So tracking will be in the presence of the error-loop and we thus deal with the full control systeem in figure 3.2.

In the equation 3.4 the transfer function from the input signal to the tracking error is given for the general system with interconnection matrix M. We substitute every entry of the matrix with the equations 3.6 that we found for the example system. The resulting transfer function is the sensitivity function for the example in figure 3.2, and is as

$$e = \frac{1}{1 + (1 + \Delta_1)P_{nom}K}d. \tag{3.30}$$

Recalling section 3.3.1, the maximum amplification of the sensitivity function is the maximum error we allow for the tracking of the setpoint signal. We can state for example that we do not want this tracking error to be greater than β. In other words, if we use a norm bounded input signal $\|d\|_\infty \leq 1$, equation 3.30 will be bounded by some $\beta > 0$. This statement is also called the *performance specification.* If β is a frequency dependant function, we can define a normalizing filter function W_P, according to β like in equation 3.19. With this definition we can express our wished performance as:

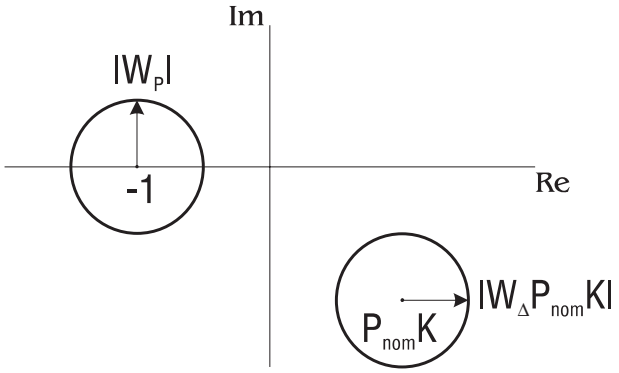

Figure 3.3: Graphical explanation of the Performance Robustness.

$$\left\| W_P \frac{1}{1 + (1 + \Delta_1) P_{nom} K} \right\|_\infty < 1. \tag{3.31}$$

Multiplying the numerator and the denomenator of this equation for $\frac{1}{1 + P_{nom}K}$ and rewriting the terms, we will obtain

$$\left\| \frac{W_P \frac{1}{1 + P_{nom}K}}{1 + \Delta_1 \frac{P_{nom}K}{1 + P_{nom}K}} \right\|_\infty < 1 \tag{3.32}$$

The left part of this equation reaches it's maximum value if Δ_1 makes the term $\left(\Delta_1 \frac{P_{nom}K}{1 + P_{nom}K} \right)$ as small as possible. It does so when Δ_1 approaches it's minimum boundary $-W_\Delta$. Then we can write (3.32) as

$$\frac{\left\| W_P \frac{1}{1 + P_{nom}K} \right\|_\infty}{1 - \left\| W_\Delta \frac{P_{nom}K}{1 + P_{nom}K} \right\|_\infty} < 1 \tag{3.33}$$

For the system to be internally stable we know from equation 3.26 that the right term in the denominator of this equation will allways have to be smaller than 1 and therefore the denominator will never become negative. That is why we may write this equation as

$$\left\| W_P \frac{1}{1 + P_{nom}K} \right\| + \left\| W_\Delta \frac{P_{nom}K}{1 + P_{nom}K} \right\| < 1. \tag{3.34}$$

Recall the sensitivity function, being the transfer function from the input d to the tracking error e as $S = \frac{1}{1 + P_{nom}K}$ and the complementary sensitivity function, being the transfer function from the input d to the actual system output θ, formulated as $T = \frac{P_{nom}K}{1 + P_{nom}K}$. Then we can formulate the robust performance criterion as follows

Take the weighting function W_Δ to norm the perturbation matrix Δ_1 to become normbounded with $\|\Delta_1\|_\infty < 1$. If W_P specifies the maximum allowed tracking error, then the system of which we know the sensitivity function S and the complementary sensitivity function T is stable and performs according to the specification in W_P if and only if

$$\|W_P S\|_\infty + \|W_\Delta T\|_\infty < 1 \tag{3.35}$$

This will be explained with the general example in figure 3.2. We may multiply the left and the right parts of equation 3.34 with $\|1 + P_{nom}K\|_\infty$. This is allowed because the nominal transferfunction should be stable and therefore this norm exists and will allways be greater than 0. The equation then becomes

$$\|W_P\|_\infty + \|W_\Delta P_{nom}K\|_\infty < \|1 + P_{nom}K\|_\infty . \tag{3.36}$$

The interpretation of this equation is given in figure 3.3. Explaining in words, construct two disks, one with center -1 and radius $|W_P|$ and one with center $P_{nom}K$ and radius $|W_\Delta P_{nom}K|$. Then robust performance is guaranteed if the two disks are disjoint. The two centers should be further from eachother then the sum of the two radi.

3.4 Small Gain Problem and μ-analysis

In this section the mathematical definitions and statements are generalized for MIMO systems. The definitions and Robust Control issues will be combined together in one mathematical method. With this method we will be able to analyse a closed-loop MIMO system on it's robustness and performance. For this purpose we need to define one more weighting function.

Figure 3.1 shows the general structure that was discussed before. Two filter functions W_Δ and W_P were defined to norm the disturbance loop (see eq.3.22) and to norm the tracking error (see eq.3.19) respectively.

The analysis involves the calculation of the perturbation loop through Δ_1 and an artificial loop from the tracking output to the input. To be able to do this, the input and the output should be normed. The output has allready been normed by W_P.

We only have to construct a maximum boundary function W_D on all representative input signals for all frequencies. Actually the function covers as tight as possible the set of amplitude-frequency plots of the occurring input signals d.
Now the real input signals can be represented in a new frequency independant normed input signal, if it is filtered through W_D.

By multiplication we can incorporate W_D, W_Δ and W_P in M. The system of figure 3.1 represents the system with norm bounded inputs and outputs. Figure 3.4 shows the way in which the analysis will be performed on this real model.

We take equation 3.2 for the interconnection matrix M. Suppose there are two defined block structures Δ_1 and Δ_2, which are compatible in size with M_{11} and M_{22} respectively. Then Δ_1 will represent the weighted perturbations and Δ_2 will represent an arbitrary norm bounded transfer function. The value of the ∞-norm of a matrix can be calculated and is equal to the maximum singular value $\sigma_{\max}(\Delta)$. Define a third structure as

$$\Delta = \left\{ \begin{bmatrix} \Delta_1 & \\ & \Delta_2 \end{bmatrix} : \sigma_{\max}(\Delta_1) \leq 1, \sigma_{\max}(\Delta_2) \leq 1 \right\}. \tag{3.37}$$

The set of all occurences of Δ will be called $\boldsymbol{B}_\Delta$. According to this generalisation, the set of all occurring Δ_1 will be called $\boldsymbol{B}_{\Delta_1}$ and the set of all occurring Δ_2 will be called $\boldsymbol{B}_{\Delta_2}$.

To answer the question in the first section on "how large" $F_u(M, \Delta_1)$ can get on the norm bounded set of perturbations, we calculate the complex sturctured singular value of the nominal system with regard to the perturbations.
As the normed perturbation Δ_1 deviates from zero, the matrix $F_u(M, \Delta_1)$ deviates from M_{22}. The range of values that $\mu_2(F_u(M, \Delta_1))$ takes, on is intimately related to $\mu_\Delta(M)$.

If the deviations in $F_u(M, \Delta_1)$ are called Δ_2 then the above statement can be seen as closing the loop with Δ_2 and M, as showed in figure 3.4.

We know that $\|\Delta\|_\infty < 1$ and that for the LFT to be well posed we need $\mu_{\Delta_1}(M_{11}) \leq 1$. This statement is equal to Theorem 3.23, but now for MIMO systems.
Robust performance will need the error of the perturbed system to be norm-bounded. Or in formula: $\mu_\Delta\left(F_u(M, \Delta_1)\right) \leq 1$. The next theorem combines the two constraints of the design problem, as stated in the beginning of this chapter.

For all $\Delta \in \boldsymbol{B}_\Delta$, the loop shown in figure 3.4 is well-posed, internally stable and $\|F_u(M, \Delta_1)\|_\infty \leq 1$, if and only if

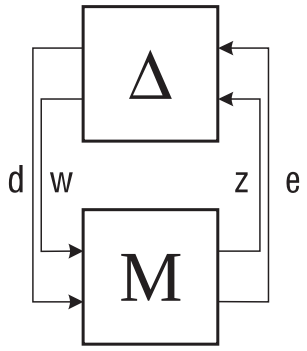

Figure 3.4: *Mathematical interpretation of robust performance analysys on a normalised system using μ-analysis.*

$$\mu_{\Delta}(M) < 1 \quad \Longleftrightarrow \quad \begin{cases} \mu_{\Delta_1}(M_{11}) < 1, \quad \textit{and} \\ \max\limits_{\|\Delta_2\|_\infty < 1} \mu_{\Delta_2}(F_u(M, \Delta_1)) < 1 \end{cases} \tag{3.38}$$

It means that if the structured singular value of the normalised system with interconnection matrix M is less than 1, we know that the system is stable and that it performs according to the constraints, under all disturbances and perturbations.

3.5 Conclusions

An overview has been presented of the aims of robust control. It explained what the rest of the report tries to achieve. That is to analyse a controller on *performance robustness.*

This chapter will end with concluding remarks on the issues of the preceding sections. These remarks should be understandable, also for the reader with less theoretical insight.

Robust performance problems can be considered as constrained minimization problems. The constraints come from an internal stability requirement and the object we seek, to minimize the infinity norm (read maximum occuring error) of some closed-loop transfer function.

Most real life systems contain several internal closed loops. This means that certain inputs depend on certain outputs.
First we want all these loops to be stable. In the sence of robust stability the focus is especially on the loops that are perturbed with disturbance or uncertainty or time-variance. If the loop-gain of such a perturbed loop is greater than 1, it means that some signal entering the loop is being amplified every time it walks through the loop once. This causes instability. So under all perturbations the loop-gain should

be smaller than 1. This is stated by theorem 3.23

In the discussion on robust performance we demand first the system to be internally stable. Then we seek the best controller that causes the error signal to stay below a certain boundary. The error signal tells us how far away the output of the system is from the desired output. A constraint on the error called the *performance specification* allowes a maximum value for this signal. The design involves a tightening of the performance specification, while the system has to remain stable.

These two constraints combined are formulated in Theorem 3.4. It poses one mathematical tool to analyse robustness and performance. We will use this tool later on in the MATLAB μ-tools software to do the job.

Chapter 4

The Bosch SCARA Interconnected

Let us recapitalize the control objective of this report. The horizontal movements of the Bosch SCARA have to be controlled. Under all perturbations, the system has to be stable and we like the performance to be as good as possible and thus the error to stay below a certain boundary. In the last chapter mathematical methods were discussed to analyse a controller on the performance specifications from the designer.

In this chapter we will prepare the model of the Bosch SCARA for the so called μ-analysis and the development of a robust controller. This includes error extraction, state space description and an interconnection scheme of all the well-known parts that have to be fit in the matrix M. In the first section the assembly of the interconnection matrix will be considered in more detail. This gives a better insight of the aim of the rest of the chapter. The next sections will, step by step, construct the structure proposed in the first section. In the final section there will be a state-space description packed in a SYSTEM matrix, compatible with the μ-analysis toolbox of MATLAB.

In the next chapter we will use the resulting model to analyse some controllers, making use of MATLAB, and to show how a robust controller can be calculated.

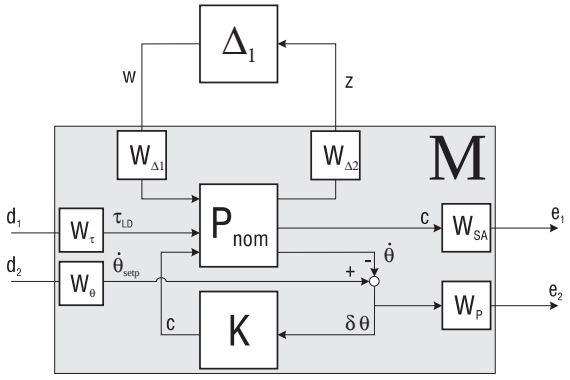

Figure 4.1: *General construction of the nominal interconnection matrix with the weighting functions.*

4.1 Structure of the Interconnection Matrix

4.2 Weighting function

In the last chapter, the general perturbed feedback system was discussed. Recall figure 3.1 to see the model we want to develop. In that model all inputs and outputs are normalized. In sections 3.3.2, and 3.3.3 two filters W_Δ and W_P were introduced to norm the perturbations and the tracking error respectively. Also the filter for the input signals W_D was discussed. The filters will be incorporated in the interconnection matrix. W_D will be split up into W_τ for the disturbance torque and $W_{\dot{\theta}}$ for the velocity setpoint.

In this way we get a feedback system that is built like in figure 4.1. Apart from the perturbation matrix Δ_1, of which we only know the norm and the structure, the model is white-box and thus called the nominal system. The nominal model is denoted by the interconnection structure M and contains everything inside the gray area.

In figure 4.1, e is the scaled output error, τ_{LD} is the disturbance torque input and $\dot{\theta}_{\text{setp}}$ is the command signal. The vector with the normalized external inputs on the system is denoted by d. Recall that d holds the inputs of the disturbance torque and of the command signal. They are filtered to become representative signals: inputs with a flat spectrum and an energy contents of 1.

W_P is the normalizing function for the tracking error. The function represents the performance specification. Iteratively, the filter W_P can be scaled up and down to tell how good the performance can be under all perturbations. Therefore a μ-analysis is performed after in every step and the filter is adapted according to the results, until maximum performance is obtained under the conditions.

W_Δ is the normalizing function for the perturbations on the system. In the case of the Bosch SCARA, W_Δ is a structured diagonal matrix containing scalars with the maximum bound of the perturbations. This structure is a result from the structure of Δ_1 which will be explained in section 4.5. As a result the weighting functions W_{Δ_1} and W_{Δ_2} in figure 4.1 can be wrapped together in one function called W_Δ.
Note the frequency independance of the perturbations. If were frequency dependant, W_Δ should be the matrix with frequency functions denoting the maximum boundary curve along the frequency axis, however no frequency dependance was found in chapter 2.

W_C is a weighting function for the second output of the system. This output represents the setpoint to the amplifier system of the Bosch SCARA. The weighting function transferres the signal to a function that has to stay below the norm to be in the range of the AD-converter.

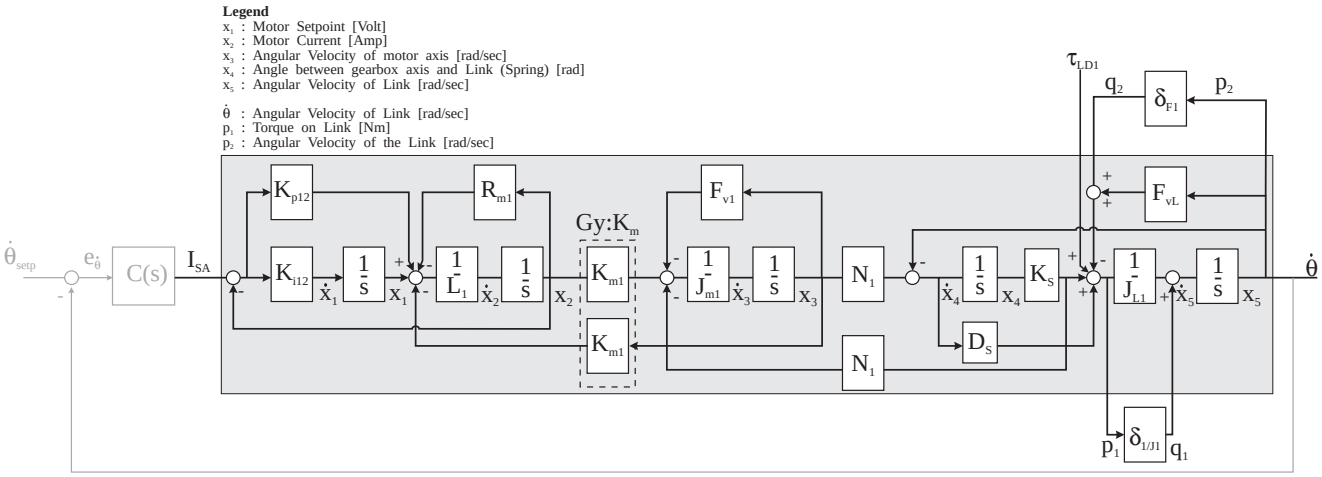

Figure 4.2: *Derived block diagram of the servo with amplifier of the first axis.*

4.3 Extracting Disturbances from the Nominal Joint Models

Chapter 2 discussed all important and relevant perturbations that influence the system. It was concluded that perturbations on the inertia and on the viscous friction are the parameter perturbations to consider, and that the independant disturbance torque τ_{LD} is also taken into account.

Figures 4.2 and 4.3 show the two separate joint models. The grey areas surround the nominal elements of the system, whereas δ_F and $\delta_{1/J}$ are the perturbations on the viscous friction and on the inertia respectively.

The model will be explained briefly again. In the left of the grey area, where the command input enters the nominal model, the PI current controller can be seen. Then the serial circuit of the motor resistance R_m and impendance L_m feeds the setpoint to the motor which is represented by the gyrator in the dashed box. The resulting torque drives the mechanical system with friction and inertia, both perturbed. The torque generates the motor axis velocity. After the gearbox with gear ration N this velocity results in the joint axis velocity.
Only for the first axis there exists a spring-damper system with spring constant K_S and damper constant D_S, which is accordingly connected to the mechanical link. The link has an own friction and inertia.

For the first motor axis all disturbances in the inertia and in the friction are transfered through the gearbox and added to the inertia and friction disturbances of the link.
For the second axis the inertia and friction of the link are transferred through the gearbox, back to the motor axis. As we will see when composing the weighting functions, these different ways of modeling have an immidiate impact on the values of the perturbations.

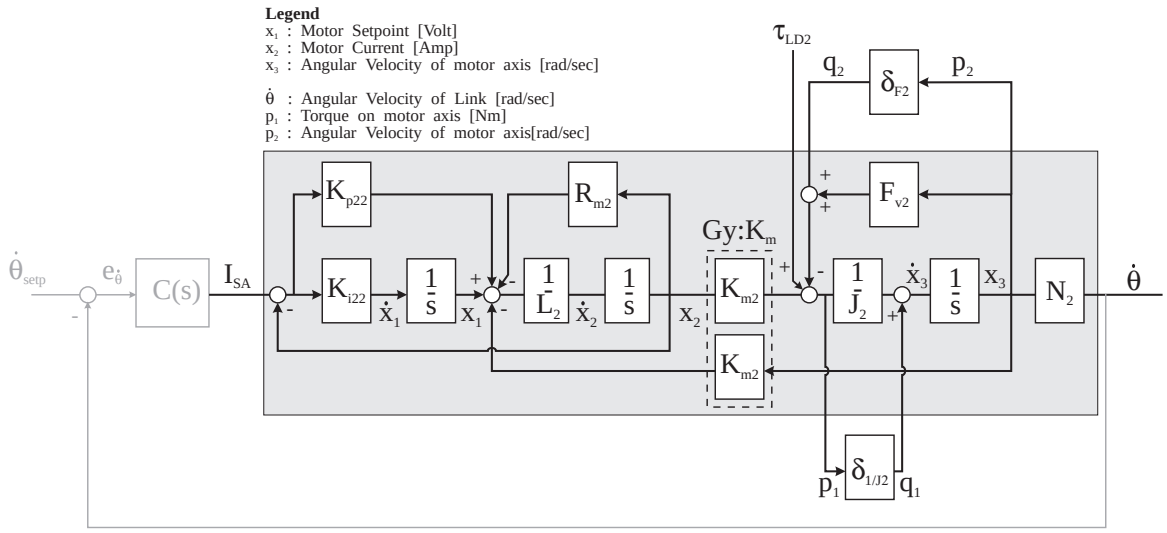

Figure 4.3: *Derived block diagram of the servo with amplifier of the second axis.*

4.4 Derivation of the State-Space System Matrices

First, the nominal system denoted by P_{nom} in figure 4.1 has to be described. To be able to make profitable use of MATLAB, the description of the model will be State-Space.

The development of State Space model theory was an important event in the late fifties. The major inspiration came from mathematicians such as Lefschetz, Pontryagin, and Bellman. Kalman deserves major credit for the state-space approach to control theory. He formulated many of the basic concepts and solved many of the importand problems.

In the world of computer controlled systems, state-space descriptions are very popular because they can be implemented in a straightforward manner. A good introduction to state-space modeling is given in [sBW90].

To derive the state-space description of the SCARA models, the output of every integration $\frac{1}{s}$ is interpreted as an internal state of the system. The input of the integration is obviously the derivative of the output.

In the figures of the models, for every state there is an indication x_i with the index i being the number of the separate state. It can be seen easily from figure 4.2 that the model of the first axis has 5 states and therefore represents a fifth order transferfunction of the system. The model of the second axis represents a third order transferfunction.

For the construction of the state-space model description of the first axis, we take a closer look at figure 4.2. The purpose is to describe all outputs as linear combinations of the states and the inputs. For

the internal description we need to describe the derived states as linear combinations of the states and the inputs as well.

For both models we will finally have the followin state-space description:

$$\dot{\boldsymbol{x}} = \boldsymbol{A}\boldsymbol{x} + \boldsymbol{B}\boldsymbol{u} \qquad \boldsymbol{Y} = \boldsymbol{C}\boldsymbol{x} + \boldsymbol{D}\boldsymbol{u} \tag{4.1}$$

with the vector $\boldsymbol{x}$ representing the states, $\boldsymbol{u}$ representing the inputs and $\boldsymbol{Y}$ representing the outputs. $\boldsymbol{u}$ and $\boldsymbol{Y}$ are constructed like

$$\boldsymbol{u} = \begin{pmatrix} I_{SA} \\ q_1 \\ q_2 \\ \tau_{LD} \end{pmatrix} \quad \boldsymbol{Y} = \begin{pmatrix} \dot{\theta} \\ p_1 \\ p_2 \end{pmatrix} \tag{4.2}$$

$\boldsymbol{A}$, $\boldsymbol{B}$, $\boldsymbol{C}$ and $\boldsymbol{D}$ are the matrices that contain the coefficients of all the linear combination equations.

For the first axis the derived states can be described by the following set of equaions.

$$\dot{x}_1 = -K_{i12}x_2 + K_{i12}I_{SA} \tag{4.3a}$$
$$\dot{x}_2 = \frac{1}{L_{m1}}(x_1 - R_{m1}x_2 - K_{p12}x_2 - K_{m1}x_3 + K_{p12}I_{SA}) \tag{4.3b}$$
$$\dot{x}_3 = \frac{1}{J_{m1}}(K_{m1}x_2 - F_{v1}x_3 - N_1 K x_4) \tag{4.3c}$$
$$\dot{x}_4 = N_1 x_3 - x_5 \tag{4.3d}$$
$$\dot{x}_5 = q_1 + \frac{1}{J_{L1}}(D_S N_1 x_3 + K_S x_4 - F_{vL}x_5 - q_2 + \tau_{LD}) \tag{4.3e}$$
$$\tag{4.3f}$$

The outputs can be described by

$$\dot{\theta} = x_5 \tag{4.3g}$$
$$p_1 = K_S x_4 + D_S N_1 x_3 - F_{vL}x_5 - q_2 + \tau_{LD} \tag{4.3h}$$
$$p_2 = x_5. \tag{4.3i}$$

Reordering coefficients and wrapping them together according to the proposed structure in equation 4.1 results in the following state matrices

$$\boldsymbol{A} = \begin{pmatrix} 0 & -K_{i12} & 0 & 0 & 0 \\ \frac{1}{L_{m1}} & -\frac{R_{m1}+K_{p12}}{L_{m1}} & -\frac{K_{m1}}{L_{m1}} & 0 & 0 \\ 0 & \frac{K_{m1}}{J_{m1}} & -\frac{F_{v1}}{J_{m1}} & -\frac{N_1 K_S}{J_{m1}} & 0 \\ 0 & 0 & N_1 & 0 & -1 \\ 0 & 0 & \frac{D_S N_1}{J_{L1}} & \frac{K_S}{J_{L1}} & -\frac{F_{vL}}{J_{L1}} \end{pmatrix} \quad \boldsymbol{B} = \begin{pmatrix} K_{i12} & 0 & 0 & 0 \\ \frac{K_{p12}}{L_{m1}} & 0 & 0 & 0 \\ 0 & 0 & 0 & 0 \\ 0 & 0 & 0 & 0 \\ 0 & 1 & -\frac{1}{J_{L1}} & \frac{1}{J_{L1}} \end{pmatrix} \tag{4.4}$$

$$\boldsymbol{C} = \begin{pmatrix} 0 & 0 & 0 & 0 & 1 \\ 0 & 0 & D_S N_1 & K_S & -F_{vL} \\ 0 & 0 & 0 & 0 & 1 \end{pmatrix} \qquad \boldsymbol{D} = \begin{pmatrix} 0 & 0 & 0 & 0 \\ 0 & 0 & -1 & 1 \\ 0 & 0 & 0 & 0 \end{pmatrix} \tag{4.5}$$

The same can be done for the model of the first axis. Notice that we now deal with three internal states. On the outside the model has as many inputs and outputs as the model of the first axis. With the aid of figure 4.3 the following equations for the states have been derived:

$$\dot{x}_1 = -K_{i22}x_2 + K_{i22}I_{SA} \tag{4.6a}$$

$$\dot{x}_2 = \frac{1}{L_{m2}}(x_1 - R_{m2}x_2 - K_{p22}x_2 - K_{m2}x_3 + K_{p22}I_{SA}) \tag{4.6b}$$

$$\dot{x}_3 = \frac{1}{J_2}(K_{m2}x_2 - F_{v2}x_3 - q_2 + \tau_{LD2}) + q_1 \tag{4.6c}$$

$$\tag{4.6d}$$

The outputs of the second axis can be described by

$$\dot{\theta} = N_2 x_3 \tag{4.6e}$$

$$p_1 = K_{m2}x_2 - F_{v2}x_3 - q_2 + \tau_{LD2} \tag{4.6f}$$

$$p_2 = x_3. \tag{4.6g}$$

From these equations also the state matrices can be constructed. They are

$$\boldsymbol{A} = \begin{pmatrix} 0 & -K_{i22} & 0 \\ \frac{1}{L_{m2}} & -\frac{R_{m2}+K_{p22}}{L_{m2}} & -\frac{K_{m2}}{L_{m2}} \\ 0 & \frac{K_{m2}}{J_2} & -\frac{F_{v2}}{J_2} \end{pmatrix} \qquad \boldsymbol{B} = \begin{pmatrix} K_{i22} & 0 & 0 & 0 \\ \frac{K_{p22}}{L_{m2}} & 0 & 0 & 0 \\ 0 & 1 & -\frac{1}{J_2} & \frac{1}{J_2} \end{pmatrix} \tag{4.7}$$

$$\boldsymbol{C} = \begin{pmatrix} 0 & 0 & N_2 \\ 0 & K_{m2} & -F_{v2} \\ 0 & 0 & 1 \end{pmatrix} \qquad \boldsymbol{D} = \begin{pmatrix} 0 & 0 & 0 & 0 \\ 0 & 0 & -1 & 1 \\ 0 & 0 & 0 & 0 \end{pmatrix}. \tag{4.8}$$

4.5 Weighting functions

In this section all the input signals and ouput signals of figure 4.2 and figure 4.3 will be normed. Simple user-defined weighting functions can do this well. Again, take a look at figure 4.1. All inputs on the grey area are normed signals. The weighting functions transfer the signals into representative signals for the internal nominal system.

Suppose an input signal $X(\omega)$ of an audio amplifier system, coming from a microphone, has to be weighted. The microphone produces a maximum output of 10 mV at frequencies above 500 Hz. Below that frequency the output will be lower and the DC-level is zero.
For this problem a weighting function of the form

$$W_{example} = 100\frac{s}{s-500}$$

transferres an input signal with flat spectrum and norm 1 into the described signal.

The weighting of perturbation, input signals and the output signals will be discussed separately.

4.5.1 Filtering the perturbations

The inertia and viscous friction appear as constant scalar parameters in the nominal models. They are assumed to be frequency independant.

To use the theory discussed in chapter 3 on parameter uncertainty, note the following. Perturbations are assumed to be scaled to 1 and the discussion only involves the magnitude and not the phase. This implies that the actual perturbation could be a circle in the origin of the complex plane with radius 1. In the case of real perturbations this implies the interval $[-1, 1]$ around the origin.

The discussion on perturbations starts with the nominal parameter and we look at the maximal extension of that value. For convenience, the nominal value should be taken in the center of the perturbation interval.

If nominal $Q_n = 10$ and the additional perturbation $\delta_Q \in [0, 3]$ then we model the perturbed parameter as $Q_n = 11.5$ with perturbation $\delta_Q \in [-1.5, 1.5]$. This way we can say that $\|\delta_Q\| \leq 1.5$ in all circumstances.

The **friction disturbances** were discussed in the first chapter. It was mentioned that it is very hard to identify accurate values for these parameters. Therefore all friction disturbances are to be taken into account. The pertubation on the viscous friction is estimated to be less then 10% under all circumstances. According to this, we construct two weighting functions W_F.

First axis		Max.Error	Units	Weighting
Friction	$F_{vL} = 95.3$	$\|\delta_F\|_\infty \leq 5.4$	$[Nms/rad]$	$W_F = 5.4$
Inertia	$J_{L1} = 8.842$	$\|\delta_{1/J}\|_\infty \leq 0.03$	$[kgm^2]$	$W_J = 0.03$
Dist.Torque	$\lim_{\omega\to\infty} \tau_{LD} = 53.32$	$\lim_{\omega\to 0} \tau_{LD} = 13.01$	$[Nm]$	$W_\tau = \frac{53.32s+13.01}{s+1}$
Input	$\|\dot{\theta}\| \leq 1.0$	$\omega_0 = 165Hz$	$[rad/sec]$	$W_{\dot{\theta}} = \frac{0.006s+1}{s+1}$
Ampl.Setp.	$\|I_{SA}\| \leq 10$		$[A]$	$W_{SA} = 0.1$
Error	According to Performance spec.		$[rad/sec]$	W_P
Second axis		Max.Error	Units	Weighting
Friction	$F_{v2} = 0.0045$	$\|\delta_F\|_\infty \leq 0.0005$	$[Nms/rad]$	$W_F = 0.0005$
Inertia	$J_2 = 4.8\,10^{-4}$	$\|\delta_{1/J}\|_\infty \leq 0.31\,10^{-4}$	$[kgm^2]$	$W_J = 0.31\,10^{-4}$
Dist.Torque	$\lim_{\omega\to\infty} \tau_{LD} = 0.46$	$\lim_{\omega\to 0} \tau_{LD} = 0.025$	$[Nm]$	$W_\tau = \frac{0.46s+0.025}{s+1}$
Input	$\|\dot{\theta}\| \leq 1.5$	$\omega_0 = 165Hz$	$[rad/sec]$	$W_{\dot{\theta}} = \frac{0.009s+1.5}{s+1}$
Ampl.Setp.	$\|I_{SA}\| \leq 10$		$[A]$	$W_{SA} = 0.1$
Error	According to Performance spec.		$[rad/sec]$	W_P

Table 4.1: *The Weighting Functions and Nominal Parameter Values*

The model of the first axis contains two viscous frictions. F_{v1} is the friction of the motor, F_{vL} is the friction of the rest of the link. Both parameters are assumed to have 10% perturbation at most. For conveniance the perturbation on F_{v1} can be transferred through the gearbox and can be added to the perturbation on F_{vL}. Because the viscous frictions of the second axis are wrapped together this way, equation 2.10 can be addressed to, for the transfer function. The value of the perturbation becomes

$$\delta_F = (0.1F_{vL}) + \left(0.1\frac{1}{N_1^2}F_{v1}\right). \tag{4.9}$$

The second axis is less complicated because there we only deal with one single friction parameter. With table 2.1 showing the estimated nominal friction values, the perturbation values can be calculated. The nominal parameters and values for perturbations are summed up in table 4.1.

The **perturbations on the inertia** is a collection of deviations of the nominal value. For J_{L1} the parameter unertainty is caused by the load mass m_l and the joint position of the second axis θ_2. Equation 2.11c gives the relation and table 2.2 gives an estimation of the dependance of θ_2. The minimal value is when $m_l = 0$ and $\theta_2 = \frac{1}{2}\pi$ rad. The perturbation on the inertia of the second axis depends only on the variable, uncertain load mass m_l. Equation 2.11c gives the belonging relation. Again, table 4.1 shows the values of the nominal parameters that are moved to the center of the real perturbed value. The size of the maximum error is needed to construct the weighting functions W_J.

Care has to be taken to calculate the error value of the parameter perturbation on the inertia. Note that in the model the parameter is below the fractional line and we add a linear additional perturbation with the

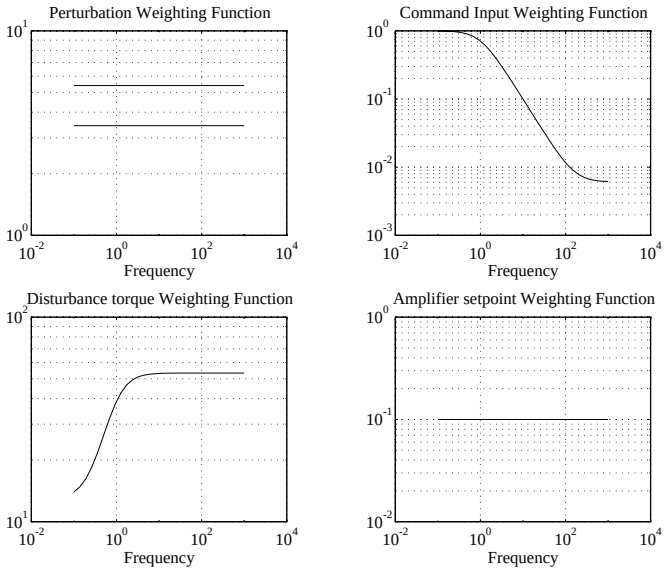

Figure 4.4: *a Plot of the Weighting Funcions for the model of the first axis, against the Frequency.*

fraction. So for the first axis,

$$\frac{1}{J_{\max}} = \frac{1}{12}, \quad \frac{1}{J_{\min}} = \frac{1}{7} \tag{4.10}$$

and with this, the maximum size of the error is half the distance between the boundaries:

$$\|\delta_{1/J}\|_\infty = \frac{1}{2}\left(\frac{1}{7} - \frac{1}{12}\right). \tag{4.11}$$

J_{nom} should have the value at which $\frac{1}{J_{nom}}$ is centered in the perturbation interval. So

$$\frac{1}{J_{nom}} = \frac{1}{12} + \|\delta_{1/J}\|_\infty \quad \Rightarrow \quad J_{nom} = \frac{12}{1 + 12\|\delta_{1/J}\|_\infty}. \tag{4.12}$$

For the implementation in the interconnection scheme as proposed in the first section of this chapter, a diagonal matrix W_Δ is being constructed according to

$$W_\Delta = \begin{pmatrix} W_F & 0 \\ 0 & W_J \end{pmatrix}. \tag{4.13}$$

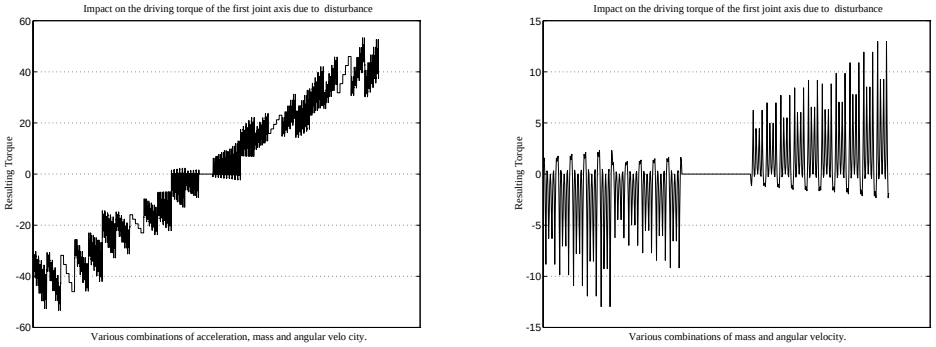

Figure 4.5: *Test in search of the boundaries of the disturbance torque of the first axis for accelerations between -10 and 10 rad/s^2 on the left and for no accelerations on the right.*

4.5.2 Weighting the independant input signals

There are two independant inputs that act on the nominal system. One is the demanded setpoint for the joint velocity, the other is the disturbance on the torque. From the μ-analysus point of view, the input signals will have to be normed and will have to have an energy contents of 1. The construction of the accuate filters that do this, is the goal of this section.

The **disturbance torque** has a static and a dynamical part. The static part is caused by the statical friction (stiction) of the motor. For the first axis this friction, like the viscous friction, is transferred through the gearbox. There is no importand need to do this, but it gives a better relational impression against the viscous friction disturbance.
The dynamical part of the disturbance torque is due to the mechanical cross-coupling between the links. Section 2.3.3 discussed this dynamical disturbance.
The weighting filter, W_τ, for the disturbance torque will be a tight maximum fit of the functions.

With equations 2.11b, 2.5 and 2.7 the dynamical disturbance torque, caused by the cross-coupling between the two axes becomes

$$\tau_{LD1} = (3.18 + m_l L_2 (L_2 + L_1 \cos(\theta_2)))\ddot{\theta}_2 - (1.68 + m_l L_1 L_2) \sin(\theta_2)(2\dot{\theta}_1\dot{\theta}_2 - \dot{\theta}_2^2) \quad (4.14)$$

$$\tau_{LD2} = N_2(3.18 + m_l L_2 (L_2 + L_1 \cos(\theta_2)))\ddot{\theta}_2 + (1.68 + m_l L_1 L_2) \sin(\theta_2)\dot{\theta}_1^2. \quad (4.15)$$

A lot of states and parameters influence the torque. To get an impression of the size of this disturbance, all combinations of all boundaries of the terms in the above equations are substituted. The values for the boundaries were discussed in chapter 2. In MATLAB this is easily done. For every variable 5 points are picked from the minimum to the maximum boundary. The result is plotted in figure 4.5. The script in MATLAB is included in appendix 7.2

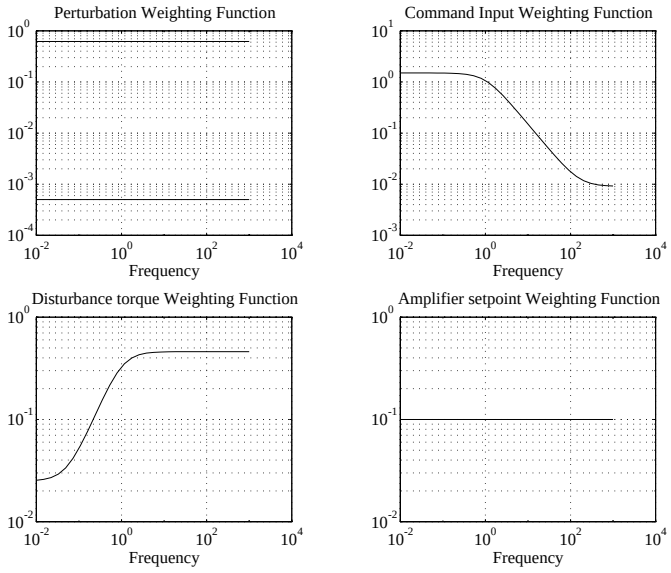

Figure 4.6: *a Plot of the Weighting Funcions for the model of the second axis, against the Frequency.*

In the sence of μ-analysis in the next chapter, we try to get a weighting function that accurately norms the disturbance in the frequence spectrum. Fast change in setpoint results in accelerations on the joint axes. Slow changes result in small accelerations. Therefore two plots are presented in figure 4.5. The left plot allowes accelerations up to 10 rad/s^2 and the right plot allowes no acceleration. This is equivalent with the high frequency setpoints respectively low frequency setpoints.
When velocities and accelerations are low, stiction plays an important role. Therefore these disturbance torques are only accounted for in the low frequency area. The perturbing static friction signals of the motor are summed op in table 2.3.

This investigation can be done for the second axis, too. It will result in the values, presented in table 4.1.

The weighting of the **setpoint** input, W_θ, is based on the set of arbitrary command inputs that is representative for the use of the robot. Because the software that will control the robot will use a sample time of 3 ms, the bandwidth of the command signals is not allowed to extend 165 Hz. Furthermore the maximum allowed value for the command signal will assumed to be 1.0 rad/sec for the first axis and 1.5 rad/sec for the second.
This results in the weighting function as in Table 4.1.

4.5.3 Norm for the performance indicator.

Two final weighting function have to be constructed. The first one is the filter for the **system error**, W_P. The policy here is somewhat different than for the input signals.

With the weighting of the error, the constraints for the μ-analysis are set. If the constraint is too stringent for the perturbed system, no satisfying controller will be found. On the other hand, we could set the weighting too loose and then find a controller (or a set of controllers) that are very conservative and perform poorly. Always the filter is small for high frequencies. This way large errors are allowed when the frequency is high.

In the next chapter we will try different weightings for the error, and analyse some controllers with the Performance Specification.

Finally the **amplifier setpoint** c has to be weighted. Therefore the weighting function W_C is created. Because the output of the DA- converter is limited to the interval $[-10, 10]$ Volt, the function represents the scalar 0.1. In the allowed interval, we know that $\|c\| \leq 1$.

4.6 Construction of the interconnection matrix

In this last section the construction of the interconnection matrix M is discussed. In figure 4.1 the gray area covers everything that has to be included in M.

In MATLAB, MIMO transfer functions are often represented by state space matrix description. To bo able to hold a complete system description (the state-space matrices A, B, C and D), the matrices are packed together in a SYSTEM[1]-matrix. The structure of a SYSTEM matrix M is as follows:

$$M := \left(\begin{array}{c|c} A & B \\ \hline C & D \end{array}\right). \tag{4.16}$$

The next sequence of MATLAB commands are the instructions to build the SYSTEM matrix. It is assumed that the variable `K` contains the system matrix that represents the controller.

At first the characteristics of the performance weighting filter are defined. Then the other filter functions are defined. The command `nd2sys` transforms a numerator - denomerator description of a function into a SYSTEM matrix. Then the square perturbation weighting function W_Δ is constructed according to the structure in equation 4.13. Finally the script `sysic` constructs the SYSTEM matrix M that represents figure 4.1.

```
W_del_F  = 5.4;
W_del_J  = 0.03;
W_tau    = nd2sys([53.32 13.01],[1 1],1);
W_inp    = nd2sys([1 165],[1 1],1/165);
W_SA     = 0.1;
W_del_J  = nd2sys([1 100],[1 1000],160);
```

[1] See the μ-tools manual for a full introduction on CONSTANT-, VARYING- and SYSTEM matrices.

```
 W_del_Fv = nd2sys([1 100],[1 1000],0.18);
 W_p      = nd2sys([1 W_p_z],[1 W_p_p],W_p_k);
 W_del    = daug(W_del_J,W_del_Fv);

 systemnames      ='ol W_del W_p W_tau W_inp W_SA';
 inputvar         ='[ pertin{2} ; tau_LD ; dist ; control ]';
 outputvar        ='[ W_del ; W_SA ; W_p ; W_inp - ol(1) ]';
 input_to_W_tau   ='[ tau_LD ]';
 input_to_W_inp   ='[ dist ]';
 input_to_ol      ='[ control ; pertin ; W_tau ]';
 input_to_W_del   ='[ ol(2:3) ]';
 input_to_W_p     ='[ W_inp - ol(1) ]';
 input_to_W_SA    ='[ control ]';
 sysoutname    ='ic';
 cleanupsysic  ='yes';
 sysic;                  % Creates the open loop structure

cl = starp(ic,K,1,1);    % Connects the controller.
```

The commands will result in the interconnection scheme, presented by the following SYSTEM matrix.

```
seesys(ic,'8.1f')

     0.0  -227.0     0.0     0.0     0.0     0.0     0.0     0.0 |      0.0     0.0     0.0     0.0   227.0
   666.7 -1913.3  -160.0     0.0     0.0     0.0     0.0     0.0 |      0.0     0.0     0.0     0.0   946.7
     0.0    22.3    -0.1-57688.8     0.0     0.0     0.0     0.0 |      0.0     0.0     0.0     0.0     0.0
     0.0     0.0     0.0     0.0    -1.0     0.0     0.0     0.0 |      0.0     0.0     0.0     0.0     0.0
     0.0     0.0     0.1  9090.9   -10.8     0.0     0.7     0.0 |      1.0    -0.1     6.1     0.0     0.0
     0.0     0.0     0.0     0.0     7.7    -0.6     0.0     7.7 |      0.0     0.0     0.0    -0.0     0.0
     0.0     0.0     0.0     0.0     0.0     0.0    -1.0     0.0 |      0.0     0.0    -6.3     0.0     0.0
     0.0     0.0     0.0     0.0     0.0     0.0     0.0    -1.0 |      0.0     0.0     0.0    -1.0     0.0
-------------------------------------------------------------------|-------------------------------------
     0.0     0.0     0.0  2400.0    -2.9     0.0     0.2     0.0 |      0.0    -0.0     1.6     0.0     0.0
     0.0     0.0     0.0     0.0     0.0     0.0     0.0     0.0 |      0.0     0.0     0.0     0.0     0.0
     0.0     0.0     0.0     0.0     0.0     0.0     0.0     0.0 |      0.0     0.0     0.0     0.0     0.1
     0.0     0.0     0.0     0.0    -0.0    -7.7     0.0    -0.0 |      0.0     0.0     0.0     0.0     0.0
     0.0     0.0     0.0     0.0    -1.0     0.0     0.0    -1.0 |      0.0     0.0     0.0     0.0     0.0
```

This matrix thus holds the nominal normed model characteristics of the first joint of the Bosch SCARA. For the second axis the same procedure can be followed. In the next chapter we will use these matrices to analyse the system on it's robustness in stability and performance.

Chapter 5

Designing the Robust Controller

The point has arrived where a suitable model of the real system is available for the theory of chapter 3 to be applied. Based on this theory, the system can be analysed on it's stability and performance if it suffers from perturbations. For that purpose some commands are available in the μ-tools package of MATLAB.

First an introduction on different methods for calculating a robust controller is given. One method is proposed to be used in this report. A μ-analysis on stability and performance is applied on the system with the unity controller. This is followed by the analysis of the system, fed back with a H_∞ controller.

Finally an explanation is given of the use of the design and analysis interface that is developed specially for the purpose of the application on the SCARA robot. Everytime when a command of the μ-toolbox is introduced throughout this chapter, the use of the command will be explained briefly. No separate chapter or section is devoted to this. For more information, the μ-analysis and synthesis toolbox guide is referred to.

This chapter will conclude with a control scheme for all models in the modelset. With this a description on the performance is immidiately available.

5.1 Design Strategy

Several methods are available for robust control design. Four of them will be discussed in this section. For clearity, every subsection is devoted to a method.

Besides these methods it is of course always possible to synthesize a control scheme, using another method, and to analyse the maximum performance. In the last section this method is mentioned once more.

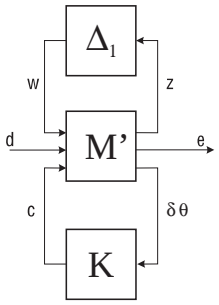

Figure 5.1: *The block diagram for calculating a H_∞ Controller.*

5.1.1 Continuous H_∞ Control Algorithm

The `hinfsyn` command calculates the full general output feedback equations based on the interconnection structure M'. The block diagram employed can be seen in figure 5.1. M' can be seen as the structure in figure 4.1 with the controller K placed outside the interconnection matrix. For this purpose an extra input and output are present in M', compared with M.

Only for comparison, the Δ_1 block is displayed in figure 5.1. This is however not necessary because the inputs and outputs are assumed to be normed and it was assumed that $\|\Delta_1\|_\infty \leq 1$. If the Δ_1 block is left out and the inputs w and d and the outputs z and e are wrapped together, a similar set of equations as in 3.3 can be formulated, now for the controller loop. This will be called the Linear Fractional Transformation on K and M'. For this LFT an optimal controller can be found. The complete set of equations and results for the H_∞ control problem can be found in [PB89] and [GJD88]. The command `hinfsyn` finds a controller K such that the closed-loop system $F_l(M', K)$ is internally stable and $\|F_l(M', K)\|_\infty \leq \gamma$ if one exists. It is called with the sequence

```
[K,M] = hinfsyn(M',n,c,gmin,gmax,tol)
```

where the outputs `K` and `M` are the H_∞ controller and the closed-loop system and `M'` is the open-loop system. `n` and `c` are the number of inputs and outputs of the controller. `gmin` and `gmax` are the boundaries of γ and `tol` is the accuracy of the algorithm.

5.1.2 Sampled-Data H_∞ Control Algorithm

Continuous time systems where measurements are sampled and then the control signal calculated by a discrete time controller followed by a hold are termed *sampled-data* systems. Two possible approaches to the controller design are available.

Consider the system of figure 5.1, where K is now a sequence of a sampler with sampling period h, the discrete time controller and the hold device that creates the output at every sample time and that is

constant between the sampling points.

It is assumed that the input is piecewize constant and that only the sampled values of the controller input are of interest. Then there is a discrete time equivalent of the system M' and discrete-time techniques can be used to calculate a H_∞ controller.
These techniques involve the bilinear transformation

$$z = \frac{1 + \frac{1}{2}sh}{1 - \frac{1}{2}sh},$$

which maps the unit disk in the z-plane into the left-half of the s-plane for any $h > 0$. The μ-tools command to calculate the discrete time H_∞ controller is `dhinfsyn`. This approach has two potential problems. First the intersample behaviour of the system outputs is ignored and second the inputs are assumed to be piecewize constant. An alternative approach is to require that the induced norm,

$$\sup_{\omega} \frac{\|z\|_{L_2}}{\|\omega\|_{L_2}} < \gamma.$$

This will handle both the above difficulties and has been studied by Bamieh and Pearson [BJP92] along with a number of other researchers [HPK90][KSH][Toi90][Yam90]. The command `sdhfsyn` uses the same sequence as `hinfsyn` execpt that besides the `tol`, the sample period `h` and the controller delay `delay` have to be specified as parameters.

To calculate the induced norm, the commands `hinfnorm` for the purely continuous time system and `sdhfnorm` for the sampled data system are available.

```
out=hinfnorm(sys,tol)
```

calculates the 1×3 vector `out`, that is made up of a lower bound for $\|\text{sys}\|_\infty$, an upper bound for $\|\text{sys}\|_\infty$ and it calculates the frequency, ω_0, at which the lower bound is achieved. `[gaml,gamu]=sdhfnorm(p,k,h,delay,to` calculates the maximum gain from the $\mathcal{L}_2$ norm of the disturbance inputs to the $\mathcal{L}_2$ of the output errors.

5.1.3 Loopshaping using H_∞ Synthesis

A particularly straightforward method of designing controllers is to use a combination of loop-shaping and robust stabilization as proposed in McFarlane and Glover [MKG89] [MKG92]. Given a system with transfer function $G(s)$ the problem setup is given in the left of figure 5.2. The first step is to define pre- and post-compensators W_1 and W_2, so that the gain of W_2GW_1 is sufficiently high at frequencies where good disturbance attenuation is required and is sufficiently low at frequencies where good robust stability is required. The second step is to design a feedback controller, K, so that

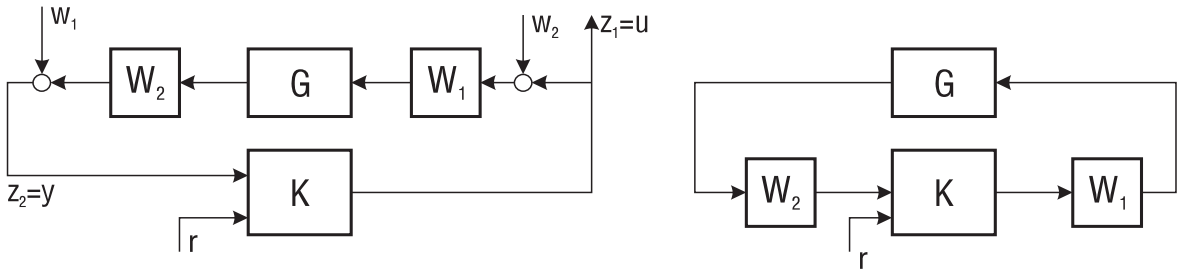

Figure 5.2: H_∞ *loopshaping standard block diagram (left)and controller implementation (right)*

$$\frac{1}{b(W_2GW_1,K)} := \left\| \begin{bmatrix} 1 \\ K \end{bmatrix} (I - W_2GW_1K)^{-1}[W_2GW_1, l] \right\|_\infty \leq \frac{1}{\epsilon}$$

which will also give robust stability of the perturbed weighted plant

$$(N + \Delta_1)(M + \Delta_2)^{-1} \text{ for } \left\| \begin{bmatrix} \Delta_1 \\ \Delta_2 \end{bmatrix} \right\|_\infty < b(W_2GW_1, K)$$

where $NM^{-1} = W_2GW_1$ is a normalized comprime factorization satisfying$N(j\omega)^*N(j\omega)+M(j\omega)^*M(j\omega) = I$. This stability margin is less than 1 and gives a good indication of robust stability to a wide class of unstructured perturbations, with values of $\epsilon > 0.2 - 0.3$ generally satisfactorily. The closed-loop H_∞ norm objective has the standard signal gain interpretation. Finally it can be shown that the controller K, does not substantially effect the loop shape in frequencies where the gain of W_2GW_1 is either low or high, and will guarantee satisfactory stability margins in the frequency region of gain cross-over. In the regulator setup, the final controller to be implemented is W_1KW_2 in the feedback configuration shown in the right of figure 5.2.

Closely related to the above problem is the approach to uncertainty using the gap family of metrics. No further attention is given to this approach here, but a reference is given to Zames and El-Sakkery [ZES80], who introduced the gap metric in control liturature. The calculation using H_∞-optimization can be found in [Geo88].

5.1.4 DK-iteration

Take the closed-loop interconnection matrix M in figure 3.1. Define a block structure Δ that is compatible to M, according to equation 3.37. As stated in chapter 3, Δ_1 corresponds to the uncertainty of the system's characteristics. Δ_2 is a fictitous uncertainty block, used to incorporate the H_∞ performace objectives on the weighted output sensitivity transferfunction. into the μ-framework.

Now, define a real matrix D with the same structure as Δ_1 :$D = \text{diag}(d_1 I, d_2 I, ..., d_k I)$, where $d_i > 0$. Enlarge this matrix to the size of Δ in equation 3.37 with a unity matrix of the size of Δ_P like $D : \text{diag}(D, I)$.

Then for each frequency we have $D\Delta D^{-1} = \Delta$ but $DMD^{-1} \neq M$. However, $\lambda(M\Delta) = \lambda(DM\Delta D^{-1}) = \lambda(DMD^{-1}D\Delta D^{-1}) = \lambda(DMD^{-1}\Delta)$. This means that the actual stability properties do not change by evaluating DMD^{-1} instead of M. So we can optimize the entries d_i in D to minimize the robust performance objective in equation 3.35. This holds in formula

$$\min_D \|DMD^{-1}\|_\infty \leq 1 \tag{5.1}$$

where D may be frequency dependant [SOBGS90]. Note that even if the uncertainty would be unstructured, the robust performance problem still has the structure $D = \text{diag}(dI_1, I_2)$, because the uncertainty feedback loop is(Δ_1, Δ_P). In this case

$$DMD^{-1} = \begin{pmatrix} M_{11} & dM_{12} \\ M_{21}/d & M_{22} \end{pmatrix}, \tag{5.2}$$

which shows that d-scaling is simple row/column scaling of the problem in an admissable way. Algorithms to optimize the scaling factors D for each frequency are well described in literature [PG89, TJD90]. Also for real-valued parametric uncertainties, algorithms have been developed. [Ter90][TJD90].

This method uses a closed-loop interconnection M in which a matrix is allready incorporated. So $M(j\omega, K(j\omega))$ is actually a function of the controller $K(j\omega)$. Using H_∞ design methods as posed in the previous section, a controller can be found, if it exists, which results in the analysis tests to hold equation 3.35.

For the structured situation, we have the design freedom of the proposed scalings left. This can be used as follows:

$$\min_{D,K} \|D(j\omega)M(j\omega, K(j\omega))D^{-1}(j\omega)\|_\infty < 1 \tag{5.3}$$

This $D - K$ iteration was suggested in [Doy84] and applied in [PG89] [DKLAP87]. Unfortunately, it is not known how to solve this minimization. An approximation to μ-synthesys involves a sequence of minimizations, first over the controller variable K (holding D fixed), and then over the D (holding the controller K fixed). It is not guaranteed that this iterating process converges.

Using the command `musynfit` of the μ-Toolbox of MATLAB, the varying variables in the D-scales can be fit in magnitude with stable, minimum phase rational functions. They are then absorbed into M

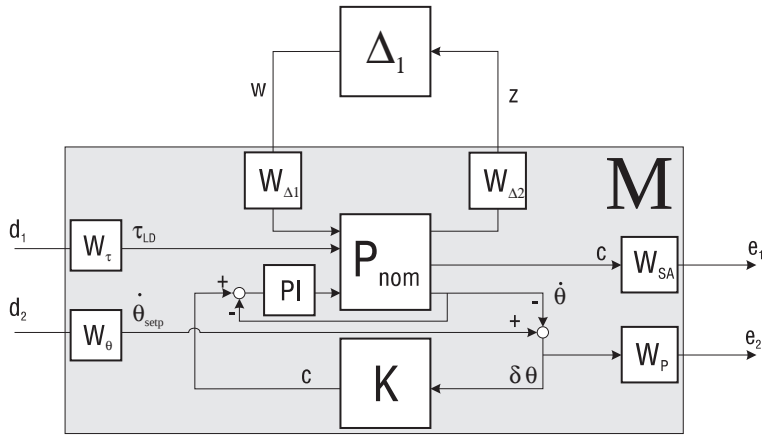

Figure 5.3: *The Existing Bosch SCARA Control System with Tacho Feedback*

for additional iterations. These scalings are used to 'trick' the H_∞ minimization to concentrate more on μ across frequency than on $\sigma_{\max}$. The syntax for `musynfit` is

```
[dsysL,dsysR]=musynfit(predsysL,Ddata,sens,blk,n,m)
```

where `predsysL` is the rational D scaling matrix from the previous iteration, `Ddata`, `sens` and `blck` are respectively the frequency varying D scales, the sensitivity variable and the Δ block structure from the previous μ analysis and n and m are, as in `hinfsyn` the number of inputs and outputs of the controller. D scaling matrices are returned. For the first iteration step for `predsysL` can be given `'first'`.

In figure 4.1 the D step in the $D-K$ iteration process can be seen as optimizing partitioning of the weighting function W_Δ in W_{Δ_1} and W_{Δ_2}. In other words, optimizing the amount of weighting on the input-side or the output-side of the perturbations. The manual of the μ toolbox is referred to for more information.

5.2 Analysis of the existing Control System with Tacho Feedback

First, the existing control system is analysed. The system with tacho feedback loops in the servo amplifiers is controlled with software, developed by Cornelis Klomp [Klo94]. On page 89 Klomp explaines the chosen value of the proportional controllers. The gains are set in such a way that the responce shows no overshoot. Care has to be taken in simulations, because the control software takes account for two slope-filters as well. They mostly determine the resulting responce for a large displacement. Figure 2.10 shows how the slope filters are implemented in the control environment.

To perform μ-analysis on the model, first a performance specification has to be defined. This is because the μ-analysis draws a plot of the robustness of the stability and performance. Without a performance

specification the μ-analysis can not tell whether the specification is obtained.

We want for example the tracking error to be smaller than 0.001 rad/sec in easy calm tracking. Typically $|W_P|$ decreases for higher freqencies. This is, because at higher frequencies larger errors do occur. In general, most control systems have a break frequency above which the system performs poorly. The according function for W_P is drawn in figure 5.4.

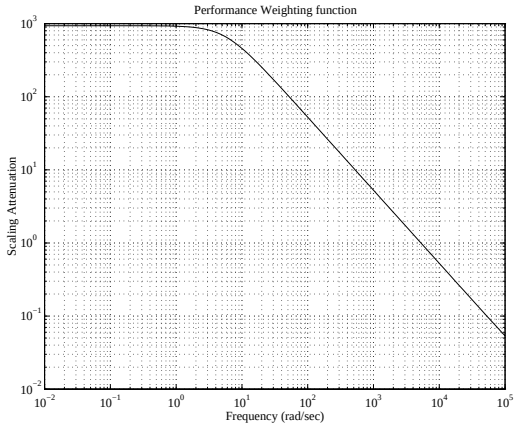

Figure 5.4: *Performance Weighting Function*

Besides a performance specification, we need a description of the model. In the end of chapter 4 the SYSTEM matrix was presented. To account for the PI-tacho controller of the original Bosch SCARA amplifier system, a tacho feedback loop will be implemented according to figure 5.3. Like in figure 5.2 the controller will be connected at the lower side of the open-loop nominal model. To connect the controller, we can make use of the command `starp` in MATLAB. Suppose `ic` is the open-loop interconnection matrix and `K` is the controller with 1 input and 1 output. Then

`cl = starp(ic,K,1,1);`.

creates a closed loop SYSTEM matrix `cl`, with 4 inputs and 4 outputs. By convention, the command `starp` will assume that the controller will use the "lowest" outputs and inputs of the open-loop system matrix. From [Klo94] the proportional parameter value of the controller of the first axis is $K_{TP1} = 46$. Now the closed-loop system can be analysed on it's Robust Performance. We will focus at a frequency range from merely steady state up to the sample time.

The Robust Stability is calculated using the following sequence of commands.

```
cl_frsp=frsp(cl,OMEGA_DK);
cl_rs=sel(cl_frsp,[1 2],[1 2]);
[rsbnds,rsdvec,rssens,rspvec] = mu(cl_rs,[1,0;1,0],'w');
vplot(plot_type,rsbnds)
```

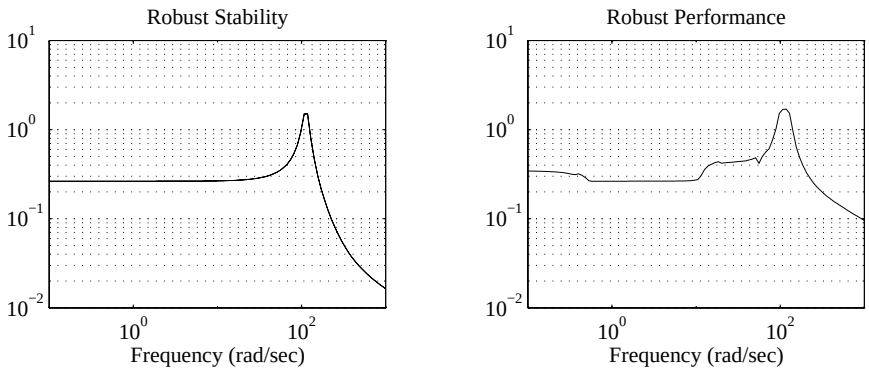

Figure 5.5: *Robust stability and performance plot of first joint axis*

First a frequency responce is generated. Then the appropriate rows and columns are selected out of the closed-loop system matrix, that corresponds with the perturbation loop. On this loop a μ-synthesis is applied.

To analyse Robust Performance the following commands are available.

```
[rpbnds,rpdvec,rpsens,rppvec]=mu(cl_frsp,BLK_DK,'wU');
vplot(plot_type,rpbnds)
```

The μ-synthesis is performed on the complete closed-loop interconnection matrix. From the results that are generated, only the robust performance bouds are plotted. That can be seen in the right of figure 5.5.

Recall from chapter 3 that the values of μ should stay below 1 for positive results. It can be seen that the robust stability plot shows a peak value above 1, at a frequency of 100 Hz. From equation 3.35 we recall that the Robust performance test is the sum of the robust stability criterion plus the nominal performance criterion. Therefore if no robust stability is guaranteed, the system will never obtain Robust performance. From this we know for sure that the peak will not disappear in the robust performance plot.
Furthermore, the performance specification acts as a weighting filter on the tracking error output of the system and has thus no influence on the internal stability. This means that if larger tracking errors would be allowed, the peak value would not disappear, and if it does, the system would resonate within the "allowed" error interval.

The poles of the closed-loop nominal system are listed below

```
spoles(cl)
```

```
-1.4872e+003
-2.7531e+002
-1.2585e+002
-2.3819e+001
-1.1484e+001+ 9.4443e+001i
-1.1484e+001- 9.4443e+001i
```

It can be seen that two imaginairy poles at -11 ± 94 are relatively close to the imaginary axis and cause poor damping of the closed-loop system. Some perturbation of the nominal system could cause the poles to drift over the imaginary axis to the right half plane in the pole-zero plot.

Only more stringent weighing functions on the disturbances could make the instability peak disappear. This means that less load mass, or a lower maximum acceleration for the second link will be allowed.

A possible explanation for the instability that occurs is that no slope filters were implemented in the nominal system. This results in steeper allowable setpoint jumps.

The controller gain for the second axis is $K_{TP2} = 42$ [Klo94]. Again the performance specification should be formulated. We take the same allowable tracking error of 0.001 rad/sec as with the first axis, see figure 5.4. and apply μ-analysis. Robust stability seems to be far below critical level 1. Even with the stringent performance specification, the robust performance plot stays below -1.

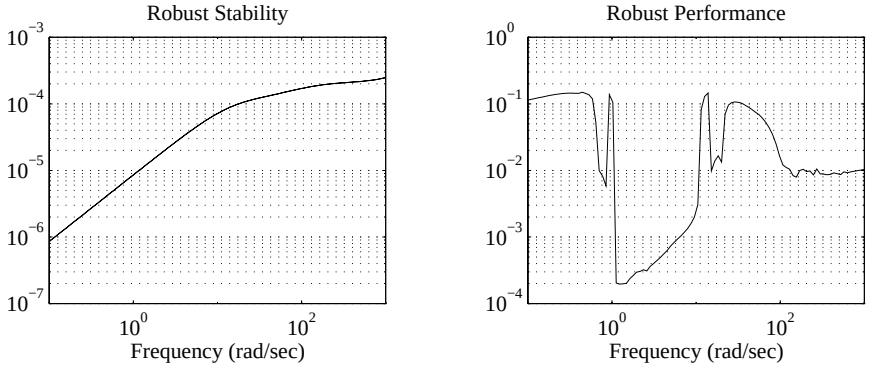

Figure 5.6: *Robust stability and performance plot of second joint axis*

The poles of the open loop system are listed below. It can be checked that there are no poles near the imaginary axis, in contrary with the system of the first joint. Therefore the μ-analysis showed good internal stability.

```
spoles(cl)
```

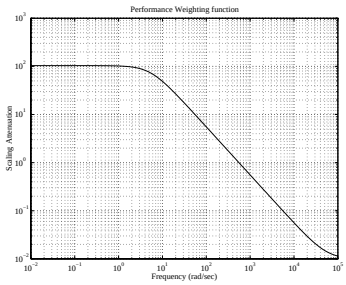

Figure 5.7: *Performance specification for the zero order controller of the first axis.*

```
-1.0793e+003+ 2.5405e+003i
-1.0793e+003- 2.5405e+003i
-1.0601e+002
-1.4776e+001
```

5.3 Analysis of a Zero Order Torque Controller

In this section we will focus on the current-controlled system as discussed in chapter 4. This is the system on which figure 4.1 applies.

It will be tried to find a control system that shows Robust performance according to a certain performance specification.

The treatment here is more a simple general example, to show how an arbitrary user-defined controller can be analysed according to Robust Control Theory principles.

Often a higher-order controller is capable of suppressing unstable modes by wisely placing or replacing poles or zeros, so that the root-locus does not driftto the left half plane too quickly. In the case of a proportional controllerno extra poles or zeros are added to the system.

At first we will focus on the first link. A tracking accuracy with a maximum allowable error of 1% upto 20 Hz will be demanded. The graphical representation of this performance specification can be seen in figure 5.7.

Suppose we would like to try a P-controller with gain-constant 120. Then this is entered in the MATLAB environment as

```
K=120;.
```

If μ-analysis is applied on the closed-loop system, the plots of figure 5.8 are generated. The peak value in the Robust stability plot is still present. This peak accounts for the peak in the Robust performance

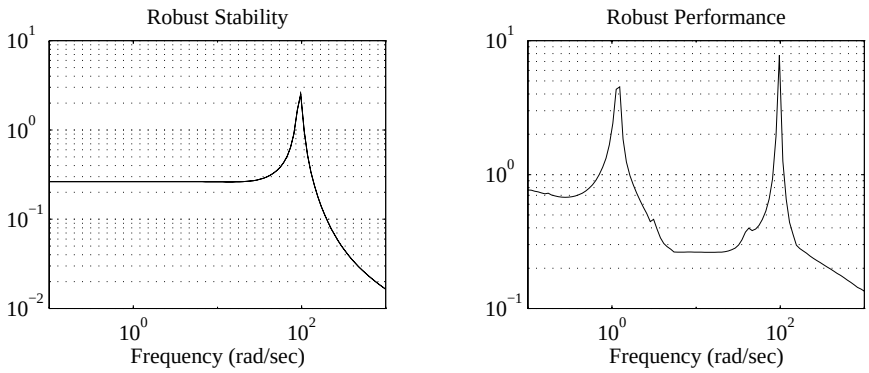

Figure 5.8: *Robust stability and performance plot of second joint axis*

plot at 200 Hz.

Let us take a look at figure 5.9. This figure shows the frequency plot of the original closed-loop system, as well as the step-responce. It also shows the Pole-Zero plot and the Nyquist plot of the original open-loop system. Original means in this case the nominal system without the weighting functions.

We can see the unstable mode in the step-responce and in the Pole-Zero plot it can be seen that two comples poles lie very close to the imaginary axis.

Apparently there will be some models in the complete set of perturbed models which will have the two poles just on the right of the axis.

The system is analysed with the same performance specification but with a proportional controller with gain 15. This results in the plots of figure 5.10.

The same analysis can be done for the second axis. First a zero-order controller with gain 2000 will be analysed. The performance specification will be more stringent than with the analysis of the first axis. The graph of W_P is presented in figure 5.11.

It can be sen from the μ-analysis in figure 5.12 that the Robust Stability can easily be guaranteed. Also Robust performance can be guaranteed because the μ plot stays below the 1-treshold. Of course this performance applies on the posed performance specification on figure 5.11.

It can be seen from the step-responce in figure 5.13 that there is an overshoot of a high-frequency resonance. This is “allowed” because the performance specification in figure 5.11 states that large errors at high frequencies are allowed.

A controller with gain 15 shows other results. Plots of the Robust stability and Robust performance are

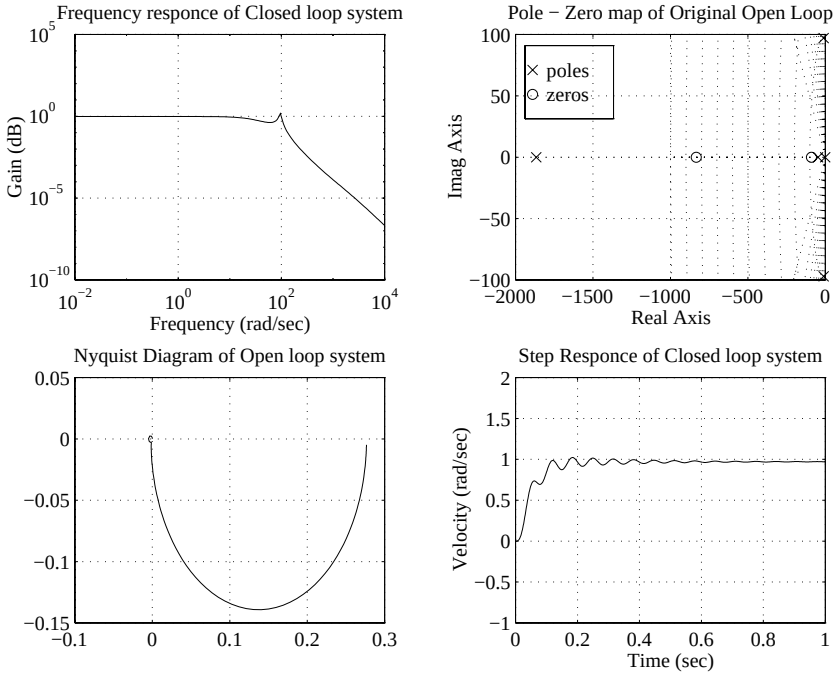

Figure 5.9: *Frequency, Nyquits, Pole-Zero and Step responce plots.*

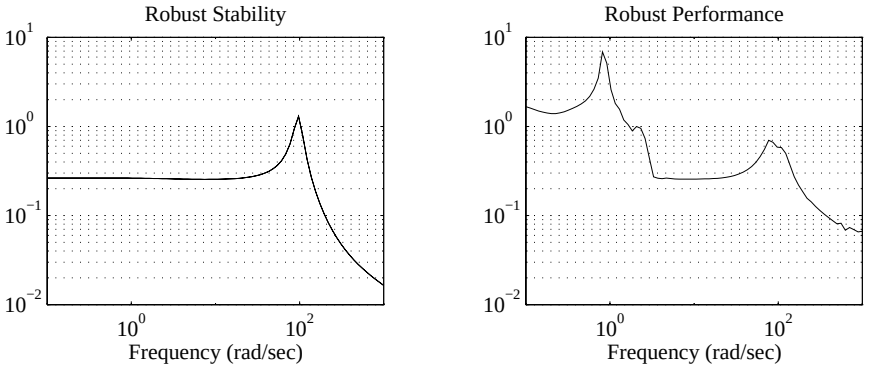

Figure 5.10: *Robust Stability and Performance plot of second joint*

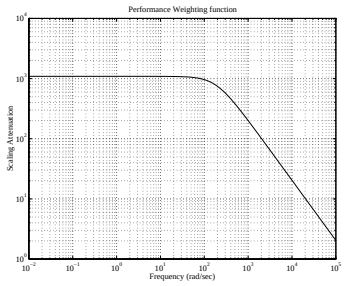

Figure 5.11: *Performance Specification*

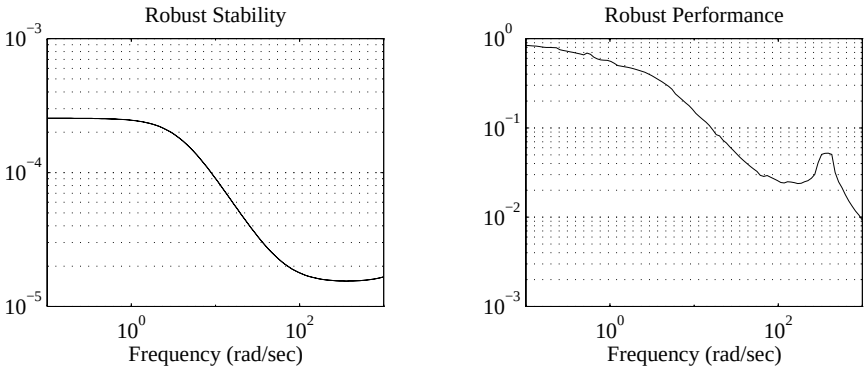

Figure 5.12: *Robust Stability and Performance plot of second joint*

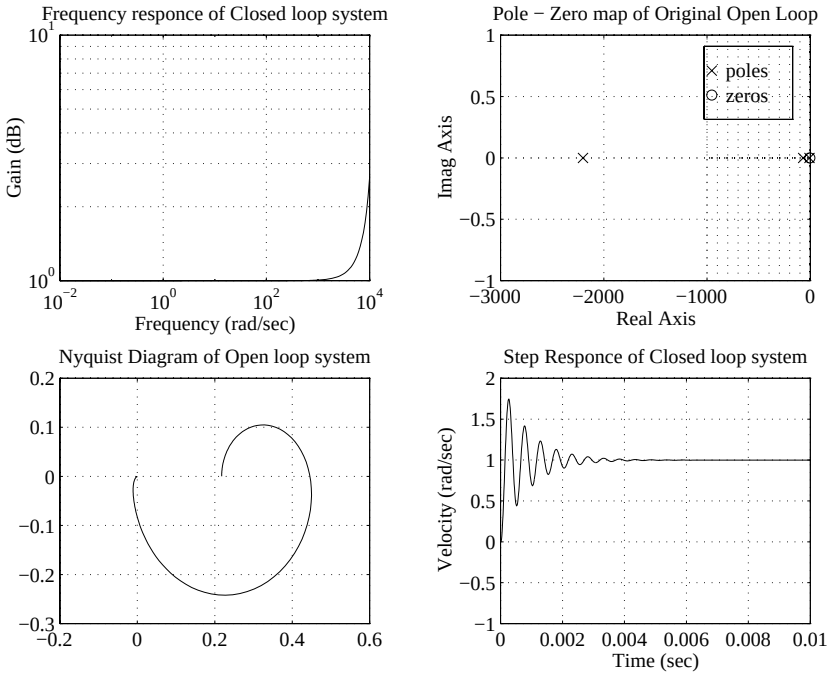

Figure 5.13: *Frequency, Nyquits, Pole-Zero and Step responce plots. Mind the transition effect of the step-responce.*

presented in figure 5.14. Note that the Robust performance analysis shows that the performance at very low frequencies is hardly guaranteed. This can be seen in the step-repsnce of figure 5.15 where a small steady-state error can be observed.

5.4 Design and Analysis of a Suboptimal H_∞ Torque Controller

In this section, two H_∞-controllers will be calculated, using the command `hinfsyn` of the μ-toolbox. This design-tool was discussed before in section 5.1.1, in the beginning of this chapter.

Again we will first have to pose a Performance specification W_P. Suppose an arbitrary specification like in figure 5.16. An error of 0.03 rad/sec is allowed in low frequencies.

With W_P being incorporated in the interconnection matrix, we can execute the command `hinfsyn`. This script runs an algorithm that tries to suppress unstabilities first and then tries to confirm to the performance specification. The command `hinfsyn` returns the controller and the closed-loop SYSTEM matrix. To get insight in the robustness of the model, again the model will be subjected to μ-analysis.

It can be seen that the system is absolutely not capable of dealing with the perturbations. The robust performance plot crosses the 1-level almost everywhere on the frequency axis. That the performance at

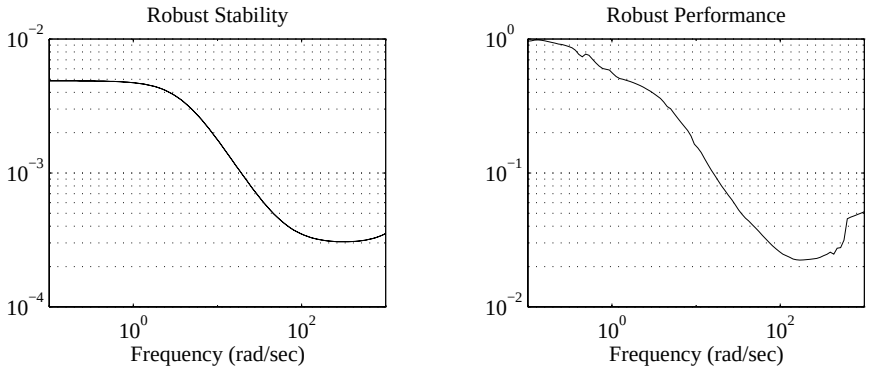

Figure 5.14: *Robust Stability and Performance plot of second joint axis*

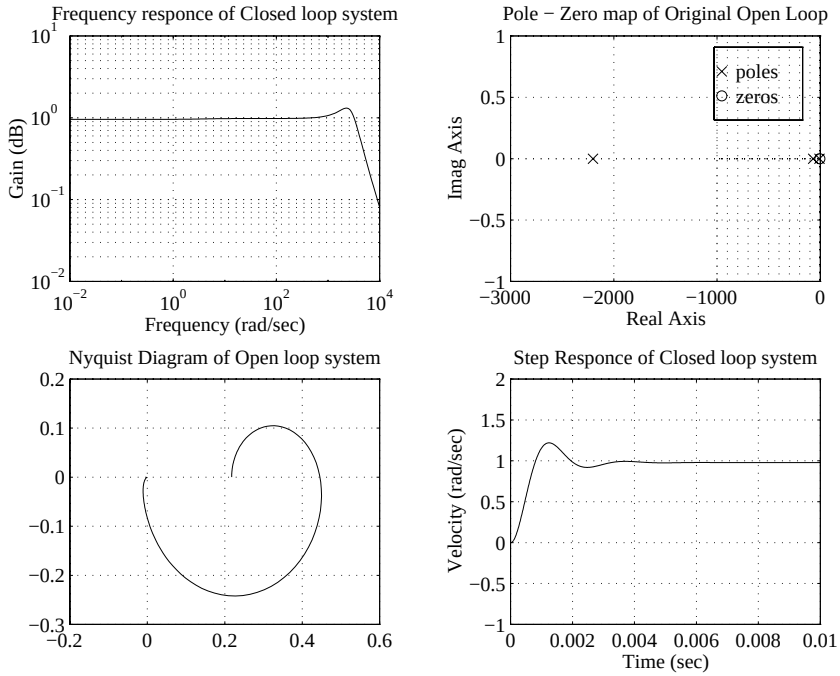

Figure 5.15: *Frequency, Nyquits, Pole-Zero and Step responce plots with* $K = 15$*. Mind the steady-state error in the step-responce.*

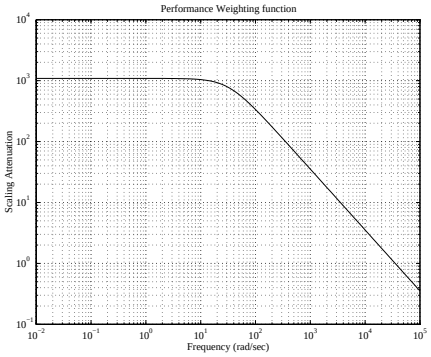

Figure 5.16: *Weighting function for the tracking error that poses the Perormance Specification*

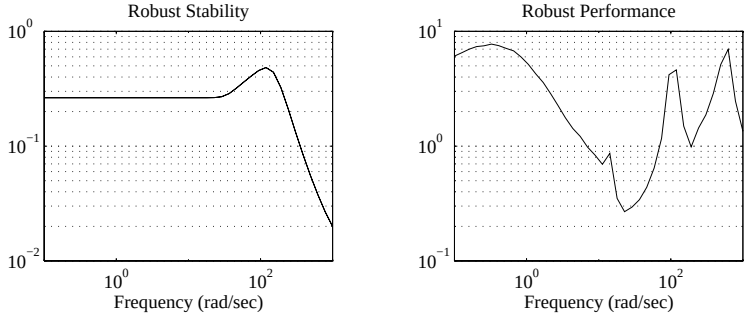

Figure 5.17: μ*-analysis on closed loop of the first joint*

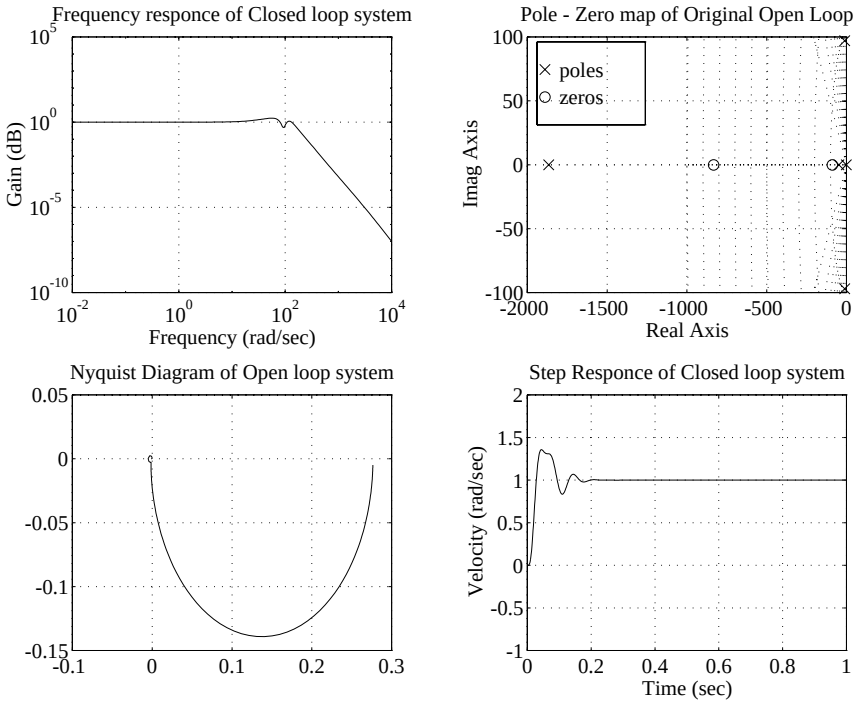

Figure 5.18: *Weighting function for the tracking error that poses the Perormance Specification*

very low frequencies is bad, can be seen from the step responce in figure 5.18. The steady state error is too large to be acceptable.

We could now loosen our performance objective and pose a less stringent criterion, but that will not help very much in the improvement of the robustness.

The only thing we can do to solve the problem is to try to decrease the size of the perturbations one way or another. First the μ-analysis is performed with $\delta_{1/J} = 0.01$, a third of the proposed value in chapter 4

From table 4.1 it can be seen that perturbations of a maximum of 0.03 $(kgm^2)^{-1}$ were allowed. This caused a 'freedom' of the inertia in the interval (7.0 12). Now the weighting function is set at 0.01. This means that J_{L1} should be in (8.08,9.65). This means a maximum allowable load mass of 3.42 kg.

With a large allowable error of 10% the μ-analysis generates the plots as displayed in figure 5.19 which indicate robust performance within a tracking-error interval of plus-minus 10%.

Finally a μ-analysis is performed on the system on which the disturbance input τ_{LD} is supposed to be zero. With W_P being 70 for low-frequencies the analysis results in the graphs of figure 5.20.

On the original system a conventional analysis of the frequency plot, step responce, Pole-Zero plot and

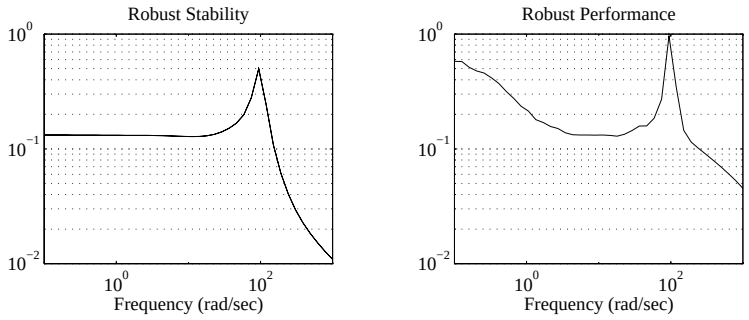

Figure 5.19: *μ-analysis on closed loop of the first joint*

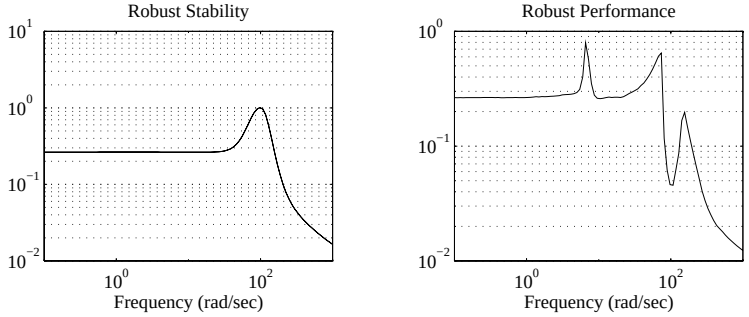

Figure 5.20: *μ-analysis on closed loop of the first joint*

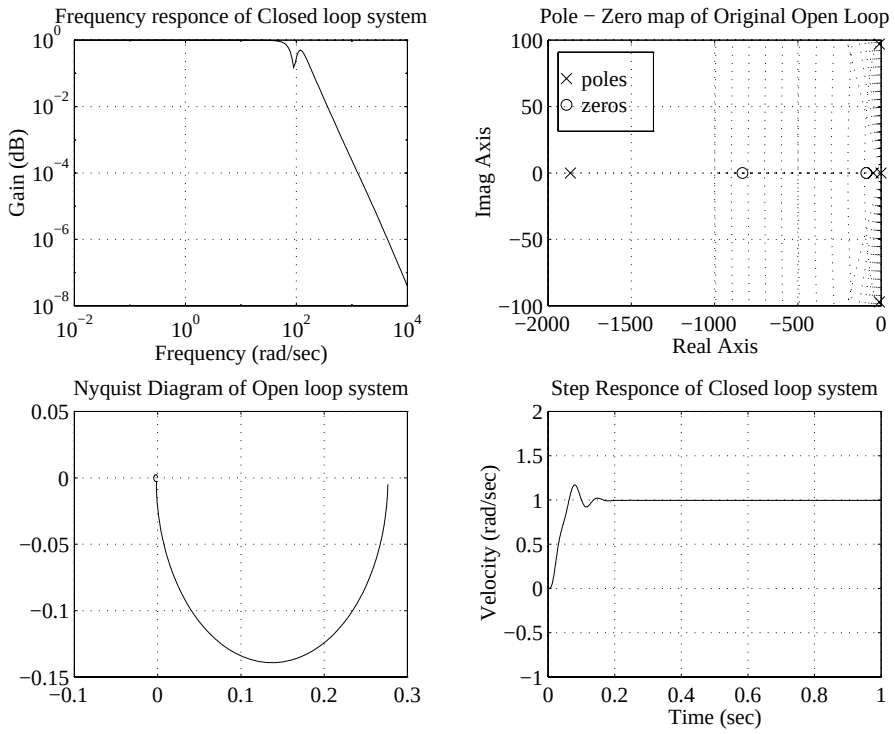

Figure 5.21: *Conventional Control analysis plots*

Nyquist diagram was peformed. This can be seen in figure 5.21.

This analysis indicates that now information on the cross-coupling is neglected by assuming two independant control systems, a lot of perturbation on the system occurs, which makes the system hard to control. In the recommandations the suggestion is posed to assume one system of two joints to solve this part of the control problem. This will not be discussed any further here.

The second axis causes less problems. The performance objective is presented in figure 5.22. μ-analysis results in the plots of figure 5.23. On the original system a conventional analysis of the frequency plot, step responce, Pole-Zero plot and Nyquist diagram was peformed. This can be seen in figure 5.24.

5.5 Interactively Developing a Controller

This chapter will conclude with the explanation of the μ-Analysis and Synthesis tool. The tool is created for general use. Any transfer function can be put in K. Then the right button has to be pressed and the user will get information on the robustness and performance of his controller, when it would be implemented in the control environment of the SCARA.

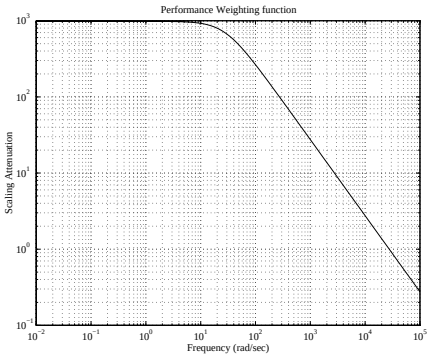

Figure 5.22: *Weighting function for the tracking error that poses the Perormance Specification*

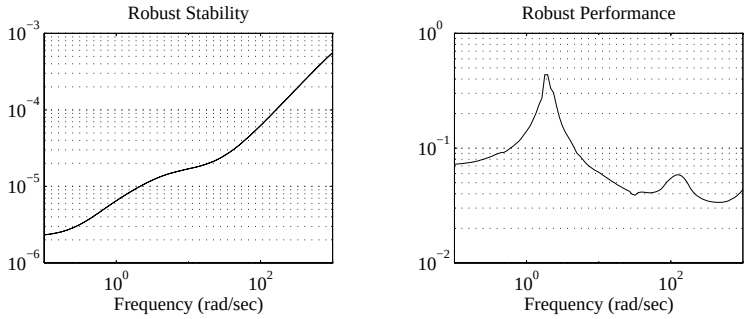

Figure 5.23: μ*-analysis on closed loop of the first joint*

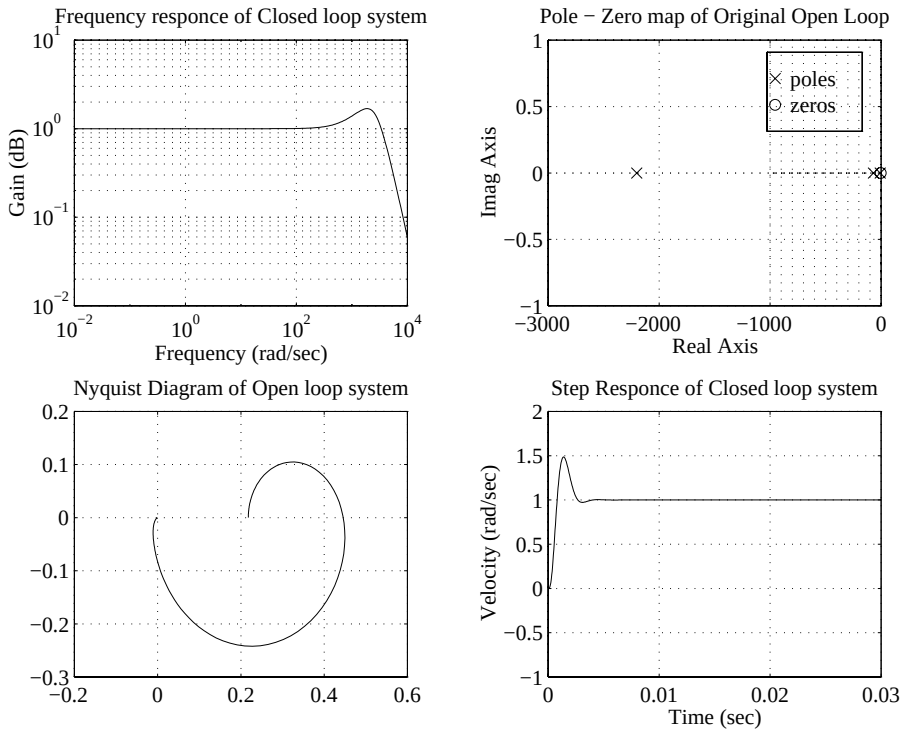

Figure 5.24: *Conventional Control analysis plots*

Figure 5.25 shows the window in MATLAB that pops up when the command `robscara` is invoced at the command line in the MATLAB Window. First the controls will be explained.

Build IC Constructs the open loop and closed loop interconnection matrix and connects the controller K that is in the environment of MATLAB.

MU CL Starts the μ-analysis of the closed loop. After the figure with the Robust stability and Robust Performance, a figure with plots that are created with the aid of conventional control theory is generated.

H-inf K Calculates a suboptimal Robust controller, making use of the μ-synthesis algorithm.

LOG radio button switches some graphs to be displayed in linear or logarithm mode.

GRID radio button that shows grid in the plots that are generated.

Tacho radio button that implements the Tacho PI-controller in the Servo Amplifier. Be aware that after this radio butto is checked, the “Build IC” command has to be invoked to generate the suitable SYSTEM matrices in the MATLAB environment.

Joint 1 Switches the joint of the Bosch SCARA that will be treated.

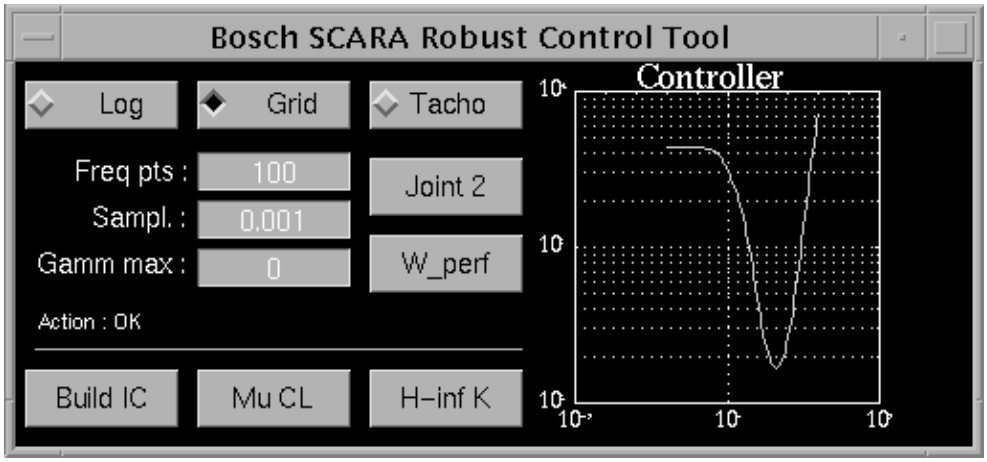

Figure 5.25: *The MATLAB Window of the SCARA control interface.*

W-perf Invokes an interactive generation and visualization of the performance weighting function that holds the performance specification.

Freq pts You can input the number of iterations the μ-analysis will perform for displaying the Robust Stability and Robust Performance plots. This is a consideration between resolution and calculation time.

Sampl. At present the number in this edit-box holds the final time of the step responce that is plotted when MU-CL is pressed.

Gamm max Starting gamma for the H_∞-controller generation.

In the right of the interface a frequency plot is plotted of the current controller in the variable K. Furthermore in the window a message is printed that informs the user what MATLAB is doing at the moment. The interface can be an information source that is very easy to use for anyone that just starts on the control laboratory.

Chapter 6

Implementation and Testing

6.1 Control Software

6.2 The Controller Recipe in C-code

6.3 A Step responce

Chapter 7

Conclusions and Recommandations

7.1 Conclusions

In the introduction of this thesis, the goal of the research was stated to design a robust controller for the Bosch SCARA by applying μ-analysis on the Linear Fractional Transformation of it's model.
For this purpose the control system environment of the first two joints of the Bosch SCARA were modelled and its parameters were identified. In chapter 4 the models were reorganized to come to the Linear Fractional Transformation of which the general setup is displayed in figure 4.1. On this transformation on a linear nominal model, by it's perturbations, μ-analysis and synthesis can be performed. In chapter 5 the system was analysed according to Robust Control Theory and for the current controlled systems a H_∞ controller was calculated. Of the closed-loop current controlled systems a μ-analysis was performed and the results drawn.

The necessity of remodelling the identified model into a LFT is a time consuming work. The problem gets even more complicated when the model contains non-linear elements. These elements then have to be considered as perturbations of the linear part of the model. An application of this kind of modelling can be found in this report. On page 60 the nonlinear friction in the servo motor was modelled as disturbance inputs to the linear system.

From chapter 5 it can be seen that if all possible perturbations on the nominal model are taken into account, the system that obtains robust performance usually shows conservative behaviour. Controllers that make the system faster can be obtained by

- Allowing larger errors on the tracking error signal. This implies that the system constraints in the performance specification become less strict. In the analysis and design tool this can be done by lowering the graph of the performance weighting filter.
- Suppressing the most sensitive perturbation to the system. With this the set of perturbed models

becomes tighter and a controller can be calculated that fits the model more appropriately. A more accurate matching of a controller to the model characteristics will improve the closed-loop performance.

- Matching the different weighting filters more accurately to the perturbations on the frequency axis. In this way, more information of the perturbations is used to improve the performance at frequencies where more performance can be gained.
- Performing a so called "D-K iteration" as explained in chapter 5. This iteration involves the optimal placement of the perturbation weighting functions at the inputs or at the outputs of the interconnection matrix. This is also discussed in the first section of chapter 4. The D-K iteration is not applied in this research.

These ways of improving a conservative system to a system that perhaps approximates a regular PI controller if the designer is lucky, is of no use when an ordinary system has to be simply controlled. Robust control theory will in practice be a very expensive tool to control a real-world system. The extensive modelling is time consuming and the advanced techniques demand from the engineer to be well aquainted with the concept. Robust control is suitable for cases in which

- The system has to be controlled within absolute maximum error boundaries. This can be the case in a coexistance of different robots in an environment or with a chemical process that has to maintain a certain setpoint. A case study on a mechanical servo system in the CD-player can be found in [SOBGS90].
- The system's performance has to be improved but there is no clue about what causes the present performance limitation. μ-analysis reveils the frequency dependance of the internal stability and of the robust performance. With the tuning of some weighting functions, the engineer can get an impression on the dependance of a specific perturbation for the performance at a certain frequency.

More than the analysis alone was accomplished with this research. In chapter 2 the complete model of the first two links of the Bosch SCARA was identified. This was structured in a step by step focus on the different parts of the control system. The amplifier system with which the servo motors are controlled was never really identified before. The model is identified empirically. The structure was derived from the circuit diagrams and parameters were estimated by applying appropriate test signals and measuring the output signals.
With this result, enough insight is given in the amplifier control system to change the characteristics. There is a tacho feedback loop present in the amplifier that is setpointed with the command signal from the DA-converter of the transputer system. This was already discussed in chapter 2. A switch has been added to the system to cut out the velocity loop and to connect the setpoint from the DA-converter directly to the current loop. In this way the setpoint represents a current and is thus proportional to the torque on the joint axis. Torque control is physically more meaningfull than velocity control. With the torque

control an impendance controller has already been developed.
Furthermore, in this thesis the analysis of the system and the design of a H_∞-controller is performed, using the μ-tools Toolbox in MATLAB. To do the μ-analysis and the μ-synthesis, an analysis and design interface script was written. With this tool, every arbitrary controller can be defined as MATLAB variable `K` and can be implemented in the Bosch SCARA model to be analysed. The μ-toolbox provides simple commands to assign dynamic transfer functions to a variable. Also the performance specification can be changed interacitively and a suboptimal H_∞-controller can be calculated. This tool can be used by anyone who wants to implement a controller in the Bosch SCARA to check the closed-loop system's robustness.

7.2 Recommandations

The advantage of robust control analysis is at the same time the main problem. Stability and a certain performance objective can be guaranteed if the analysis displays that the largest singular value of the closed-loop system stays below 1. If there is little known about perturbations, or if there are 'large' parameter uncertainties, it will be hard to achieve some interesting performance. Often the system will perform conservatively.
If, on the contrary, more is known about the system, then the maximum size of the perturbation loop might become smaller. Then more loopgain is allowed in the nominal model, by which means the performance can be improved.
In the case of the Bosch SCARA, I think, it would be interesting to consider the horizontal movement as one control problem. Most of the large disturbanced denoted by τ_{LD} will then be modelled explicitly in the nominal model. Any parameter uncertainties in the cross-coupling part could than be modelled as perturbations.

In this report the Bosch SCARA system is considered to be well-known, apart from the perturbations that were considered (friction, inertia and disturbance torques). These perturbations, however, were the largest in size, compared to other parameter uncertainty.
It seems interesting to me, to take more (most of the) uncertainties into account. The yet remaining perturbations are small, but the system could perhaps be very sensitive to one parameter deviation. That research will then give a better insight in the systems characteristics.

In chapter 5 a controller was calculated using a suboptimal H_∞-algorithm of the μ-toolbox called `hinfsyn`. The controllers all result in conservative control laws.
In the same chapter the D-K iteration procedure for designing an optimal H_∞-controller was explained. I am convinced that more performance can be gained, if the perturbation weighting filter W_Δ is devided wisely on the inputs and outputs of the system. This could perhaps be the subject of another extended research towards a H_∞ control law for the Bosch SCARA.

The μ-synthesis algorithm that calculates a H_∞ controller, always generates a controller of the same order as the interconnection matrix. The interconnection matrix is created of the nominal model with all defined weighting matrices. For the first axis the interconnection matrix has already 8 states.
It should be possible to control the system well, with a controller of at most second or third order. For this purpose a model reduction algorithm is present in the μ-toolbox. The research to the extra gained performance of a robust system when using an eighth order controller instead of a second order in different circumstances, could be interesting.

Finally, we deal with a sample and hold system in this thesis. For this type of systems, a script is available in the μ-toolbox, to create a subpotimal H_∞-controller. However, at present the algorithm that calculates the controller only deals with an interconnection matrix of which the D-matrix is zero. No outputs should be instantly dependant on one of the inputs. In our case the perturbation loop contains outputs that are proportionally related to the inputs. Therefore I could make no use of the script. It could be a valuable research to develop an algorithm that allowes the D-matrix to be non-zero.

These remarks conlude this thesis of which I had much joy in making it. Of course graduation time is often too short to go into the matter deep enough to satisfy the personal needs of the student.

Index

Amplifier Models in PSIE The Psie model of the first part of the servo amplifier is printed below.

```
** Structure and parameters of present model **
================================================
Block     Type Inputs/Comment               Par1        Par2        Par3
=============================================================================
AMPL_IN   CON                               .4400
INGANG    GEN  AMPL_IN,0.056,0              .0000       .0000       1.000
BEGIN     INF  INGANG                      -.4400       1.000      8.0000E-05
I_REG     INT  KI*BEGIN                     .0000
KI        PAR  1.3/0.028/AMPL_IN
KP        PAR  6.3/2/AMPL_IN
P_REG     VAR  KP*BEGIN
UIT       VAR  P_REG+I_REG
```

The Psie model of the second part of the servo amplifier is printed below.

```
** Structure and parameters of present model **
================================================
Block     Type Inputs/Comment                Par1        Par2        Par3
=============================================================================
AMPL_IN   CON                              7.5000E-02
INGANG    GEN  AMPL_IN,0.116,0             1.0000E-02   .0000       1.000
I_REG     INT  KI*INGANG                   -1.450
KI        PAR  2.5/AMPL_IN/0.056
KP        PAR  0.4/AMPL_IN/2
UIT       VAR  I_REG+KP*INGANG
```

Disturbance Boundary test

```
points  = 5
max_mass = 5
max_acc = 10;
% angle is in  (-0.5pi , 0.5pi)
% veloc1 is in (-1.0   , 1.0  )
% veloc2 is in (-1.5   , 1.5  )

if max_acc==0,acc(1)=0;acc_points=1; else;acc_points=points;
acc     = (-max_acc:2*max_acc/(points-1):max_acc)';end;
angle   = (-0.5*pi:pi/(points-1):0.5*pi)';
mass    = (0:max_mass/(points-1):max_mass)';
veloc1  = (-1:2/(points-1):1)';
veloc2  = (-1.5:3/(points-1):1.5)';

max_tau_1 = -100;
min_tau_1 = 100;
max_tau_2 = -100;
min_tau_2 = 100;
tau_1   = 0:points^5:1;
tau_2   = 0:points^5:1;

% i1=1;acc(1)=0;
for i1  = 1:acc_points,
for i2  = 1:points,
for i3  = 1:points,
for i4  = 1:points,
for i5  = 1:points,

adres = (i1-1)*points^4+(i2-1)*points^3+(i3-1)*points^2+(i4-1)*points+i5;

tau_1(adres) = (3.18+mass(i3)*0.355*(0.445+0.355*cos(angle(i2))))*acc(i1)-...
  (1.68+mass(i3)*0.445*0.355)*sin(angle(i2))*(2*veloc1(i4)*veloc2(i5)-veloc2(i5)^2);

tau_2(adres) = 1/101*((3.18+mass(i3)*0.355*(0.445+0.355*cos(angle(i2))))*acc(i1)-...
  (1.68+mass(i3)*0.445*0.355)*sin(angle(i2))*veloc1(i4)^2);

if tau_1(adres)>max_tau_1,max_tau_1=tau_1(adres);imax_1= [i1 i2 i3 i4 i5];end;
if tau_1(adres)<min_tau_1,min_tau_1=tau_1(adres);imin_1= [i1 i2 i3 i4 i5];end;
if tau_2(adres)>max_tau_2,max_tau_2=tau_2(adres);imax_2=[i1 i2 i3 i4 i5];end;
if tau_2(adres)<min_tau_2,min_tau_2=tau_2(adres);imin_2= [i1 i2 i3 i4 i5];end;

end;end;end;end; disp([' ',num2str(i1)]);end;
disp(['First axis: Maximum tau:',num2str(max_tau_1),' Mimimum tau:',num2str(min_tau_1)]);
disp(['Secnd axis: Maximum tau:',num2str(max_tau_2),' Mimimum tau:',num2str(min_tau_2)]);

plot(tau_1)
set(gca,'xtick',[0 1 2])
xlabel('Various combinations of mass and angular velocity.')
ylabel('Resulting Torque')
title('Impact on the driving torque of the first joint axis due to disturbance')
set(gca,'ygrid','on')
```

References

[BJP92] Bamieh and B.A. J.B. Pearson. *A General Framework for Linear Periodic Systems with Applications to H_∞ Sampled Data Control*, volume AC-29, pp.418-435. IEEE Trans. Aut. Control, 1992.

[DCIoTtT92] Allen R. Tannenbaum (University of Minnesota Doyle (California Institute of Technologie), Bruce A. Francis (University of Toronto) and John C. the Technicon). *Feedback Control Theory*. Maxwell MacMillan International, 1992.

[DH92] J. De Haas. Modelling of a scara robot. Master's thesis, Delft University of Technology, 1992. Master's thesis (in Dutch).

[DKLAP87] J.C. Doyle K. Lenz A. Packard. *Design examples using μ-synthesis: Space Shuttle lateral axisFCS during re-entry*, volume F.34 of *ASI*. NATO, 1987. *Modelling, Robustness and Sensitivity reduction in Control Systems* (Ed.R.Curtain).

[Dor89] Richard C. Dorf. *Modern Control Systems*. ISBN 0-201-54279-X. Addison Wesley Publishing Company, Inc., fifth edition edition, 1989.

[Doy84] J.C. Doyle. *Advances in Multivariable Control*. Lecture notes on the ONR / Honeywell Workshop, Honeywell, Minnesota, 1984.

[Geo88] T.T. Georgiou. *On the computation of the Gap Metric*, volume Vol II. Systems and Control Letters, 1988. pp. 253-257.

[GJD88] K. Glover J.C. Doyle. *State-Space formulae for all stabilizing Controllers that satisfy an H_∞ norm bound and relations to risk sensitivity*. Systems and Control Letters, 1988.

[HPK90] Hara and S. P.T. Kabamba. *On Optimizing the induced norm of Sampled Data Systems*. CA, american control conference edition, 1990.

[Klo94] Cornelis Klomp. *Sensor Based Fine Motion Control*. PhD thesis, Control Lab, Dept of Electrical Engineering, Delft University of Technology, 1994.

[KSH] P.T. Kabamba S. Hara. *Worst case Analysis and Design of Sampled Data Control Systems*. preprint, –.

[Mac91] J.M. Maciejowski. *Multivariable Feedback Design*. ISBN 0-201-18243-2. Addison-Wesley Publishing Company, Cambridge University and Pembroke College, Cambridge, third edition edition, 1991.

[MKG89] McFarlane and D.C. K. Glover. *Robust Controller Design, using Normalised Coprime Factor Plant Description*, volume Volume 138. Springer Verlag, 1989. Lecture notes in Control and Information Sciences.

[MKG92] McFarlane and D.C. K. Glover. *A Loops-Shaping Design Procedure using H_∞ Synthesis*, volume Vol.37 nr.6. IEEE Trans. Auto. Control, June 1992. pp. 759-769.

[PB89] Doyle K.Glover P.Khargonekar and J.C. B.Francis. *State Space solutions to standard H_2 and H_∞ control problems*, volume Vol.34 no.8. IEEE Transactions on Automatic Control, August 1989.

[PG89] A.K. Packard G.J.Balas. *MUSYN Control Software manual on μ-synthesis*, volume CA of *from Theory and Application of Multivariable Control*. Arcadia, short course edition, September 11-14 1989.

[RC94] Robust and Adaptive Control. *Design examples using μ-synthesis: Space Shuttle lateral axisFCS during re-entry*, volume Tutorial Workshop. EURACO NETWORK, 29 August - 2 Sept 1994. University of Dublin, Trinity Collega, Dublin, Ireland.

[Rie92] Theodorus A. Rieswijk. *Robot Trajectory Planning*. PhD thesis, T.U.Delft, 1992.

[Roe87] R. Roest. *Inleiding Mechanica*. Delftsche Uitgevers Maatschappij, 1987. Lecture notes.

[sBW90] Åstrom and Karl J. Bjorn Wittenmark. *Computer Controlled Systems (Theory and Design)*. ISBN 0-13-172784-2. Prentice-Hall International, Inc., Department of Automatic Control, Lund Institute of Technology, Box 118, S-221 00, Lund Sweden, second edition edition, 1990.

[Sha49] C. E. Shannon, editor. *Communications in the Presence of Noise*, volume Proc. IRE, 37 of *10-21*, 1949.

[Smi94] G.J. Balas J.J. Doyle K. Glover A. Packard R. Smith. *μ-Analysis and Synthesis TOOLBOX User's Guide*. MUSYN Inc. and The Math Works Inc., Cambridge University and Pembroke College, Cambridge, third edition edition, Januari 1994.

[SOBGS90] M. Steinbuch O.H. Bosgra G. Schootstra. *μ-Synthesis of a Flexible Mechanical Servo System*. T.U.Delft, The Netherlands, summer school on h_∞ control and robust stabilization edition, June 11-15 1990. Philips Research Laboratories & Delft University of Technology, Other Participants of S.G. Smit J.C. Terlauw N.A. Bruinsma.

[Str88] Gilbert Strang. *Linear Algebra and its Applications*. ISBN 0-15-551005-3. Harcourt Brace Jovanovich International Edition, Massachusetts Institute of Technology, third edition edition, 1988. Library of Congres Catalog Card Number: 87-083019.

[Ter90] J.C. Terlouw. *Robustness Analysis of Control Systems with Parametric Uncertainty*. TN-099/90. Philips Technical Note, 1990.

[TJD90] Fan A.L. Tits and M.K.H. J.C. Doyle. *Robustness in the Presence of Parametric Uncertainty and Unmodeled Dynamics*. IEEE Transactions on Automatic Control, 1990.

[Toi90] H.T. Toivonen. *Sampled Data Control of continuous time Systems with an H_∞ optimality criterion*, volume Rep 90-1. Dept of Chemical Engineering, Abo Academi, Finland, Januari 1990.

[Yam90] Y. Yamamamoto, editor. *A New Approach to Sampled Data Control Systems - A Function Space viewpoint with applications to tracking problems*, volume pp. 1882-1887, 1990.

[ZES80] G. Zames El-Sakkary, editor. *Unstable systems and Feedback: The Gap Metric*, October 1980. pp.380-385.